Computer Assisted Mechanics and Engineering Sciences, 4: 417–451, 1997.

Alternative displacement frame formulations in hybrid-Trefftz Kirchhoff plate p-elements

Jaroslav Jirousek* and Adam Wróblewski†
Swiss Federal Institute of Technology, LSC–DGC,
CH–1015 Lausanne, Switzerland

Bogdan Szybiński‡
Institute of Mechanics and Machine Design,
Cracow Institute of Technology, Poland

(Received December 20, 1996)

The thin plate p-elements considered in this paper are based on assumed displacement field chosen so as to *a priori* satisfy the governing Lagrange equation within the element. The required C^1 conformity is then enforced in a weak sense trough an auxiliary displacement frame defined in terms of nodal and side mode parameters. While thus far the standard approach consisted in using three parameters (one displacement and two rotations) at corner nodes and an optional number of side mode parameters associated with mid-side nodes, other alternative formulations are also possible wherein the number of corner mode parameters is either inferior or superior to three. As compared to the standard frame, such alternative formulations may exhibit some advantages and some shortcomings with respect to accuracy, convergence rate, error distribution, computational efficiency and/or ease of use. The paper surveys and critically assesses some of such formulations and reports the results of extensive numerical studies involving regular and singular plate bending applications.

1. Introduction

If, instead of the Ritz method, the Trefftz [1] method is used as a basis for the development of finite elements (FE) in solid mechanics and structural applications, the element formulation is still based on assumed displacements. But unlike the Ritz-type approach, the assumed displacements are now chosen so as to *a priori* satisfy the governing differential equations of the problem (e.g. the Lagrange equation in the case of the classical thin plate), rather than the usual conformity conditions. The interelement continuity and the boundary conditions are then enforced on the element in a weak sense. The simplest, though not unique, way to achieve this consists in the application of hybrid methods [2], where by the conformity is enforced (as in the well known hybrid-stress element approach introduced by Pian [3]) through an auxiliary displacement frame, independently defined at the boundary of the element. Various alternative formulations are also possible but comparatively less used (for a review see e.g. [4, 5]).

The standard form of the formulation known as the "hybrid-Trefftz" (HT) FE model was first applied to the development of simple and very efficient plane elasticity and plane bending h-method elements [6, 7]. The idea of forming also the p-version of the HT elements was presented for the first time already in 1982 [6], but the p-method capability was practically implemented and thoroughly studied only in 1987 [8]. Very soon it became clear that these elements are largely superior to the earlier HT h-elements and in the subsequent years the HT-elements research was focused nearly

* Professor

† Research engineer, on leave from Cracow Institute of Technology

‡ Assistant

exclusively on these p-elements. Different aspects were studied including accurate representation of curvilinear geometry [9], use of the optional special purpose functions in order to allow various geometry or load dependent singularities or local effects to accurately be accounted for without mesh adjustment [10–13], comparison of performance, accuracy and convergence properties with conventionally formulated p-elements [14, 15], error estimation and adaptivity [16–19].

Thus far in all HT thin plate p-elements use was made of a single type of displacement frame, involving three DOF (one displacement and two rotation components) at corner nodes and an optional number of hierarchical side mode DOF associated with mid-side nodes. Surprisingly, the possibility of using at element corners less or more than the three customary DOF did not attract the curiosity of research workers despite its obvious theoretical and practical interests. The aim of this paper is to fill this gap. Three alternative displacement frame definitions presenting respectively 1, 3 and 6 DOF at corner nodes, will be considered. Their advantages and drawbacks will be evaluated critically on the basis of theoretical considerations and/or numerical studies. The main aspects under consideration will be the consequences of the displacement frame definition on the accuracy, h- and p-convergence rates, error distribution, sensitivity to mesh distortion, computational efficiency and ease of use. Attention will also be paid to their capacity of representing the out of plane behaviour component in the application to thin folded plates.

2. THEORY

2.1. Theoretical formulation of the HT plate element

The standard form of the assumed displacement field of the element is

$$w = \overset{\circ}{w} + \sum_{j=1}^{m} W_j c_j = \overset{\circ}{w} + \mathbf{W}\mathbf{c}\,, \tag{1}$$

where $\overset{\circ}{w}$ and W_j are known functions and c_j are undetermined coefficients. In order to satisfy the governing Lagrange plate equation

$$\nabla^4 w = \frac{p}{D} \tag{2}$$

of the classical theory of thin plates, where $\nabla^4 = \partial^4/\partial x^4 + 2\partial^4/\partial x^2 \partial y^2 + \partial^4/\partial y^4$ is the biharmonic operator, p stands for the intensity of the distributed load and

$$D = \frac{Et^3}{12\,(1-\nu^2)} \tag{2a}$$

(t — plate thickness, E — Young modulus, ν — Poisson's ratio), $\overset{\circ}{w}$ and W_j in (2) have to be chosen so that

$$\nabla^4 \overset{\circ}{w} = \frac{p}{D} \qquad \text{and} \qquad \nabla^4 W_j = 0 \qquad (j = 1, 2, \therefore, m) \tag{1a,b}$$

everywhere in the element subdomain Ω^e. From (1) the conjugate vectors of generalized boundary displacements $\mathbf{v}$ and generalized boundary tractions $\mathbf{t}$ at the element boundary Γ^e (Fig. 1) are readily derived as

$$\mathbf{v} = \begin{Bmatrix} w \\ w_x \\ w_y \end{Bmatrix} = \begin{Bmatrix} w \\ \partial w/\partial x \\ \partial w/\partial y \end{Bmatrix}, \quad \mathbf{t} = \begin{Bmatrix} S_n \\ -M_{nx} \\ -M_{ny} \end{Bmatrix} = \begin{Bmatrix} n_x Q_x + n_y Q_y \\ -n_x M_x - n_y M_{xy} \\ -n_y M_y - n_x M_{xy} \end{Bmatrix}, \tag{3a,b}$$

where (Fig. 2)

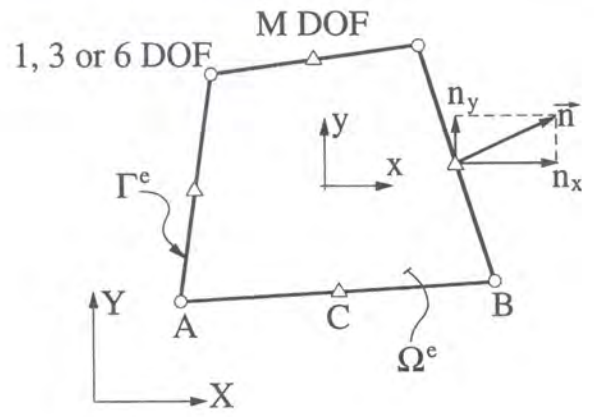

Fig. 1. Typical HT plate bending p-element with fixed number ($N = 1$, 3 or 6) of DOF at corner nodes ○ and optional number $M \geq 1$ of side-mode DOF alloted, formally, to mid-side nodes △

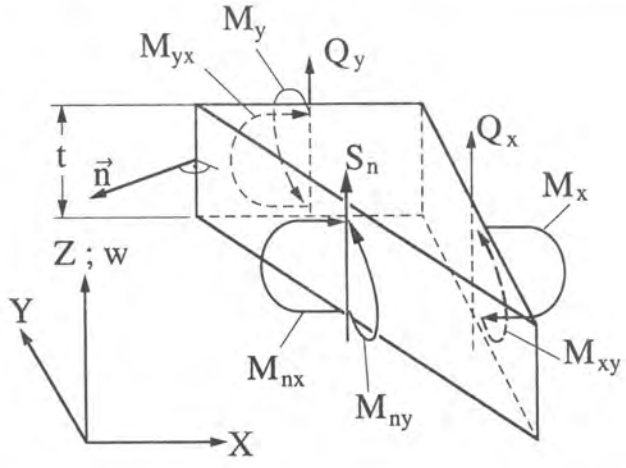

Fig. 2. Sign convention of internal forces M_x, M_y, M_{xy}, Q_x, Q_y and of boundary tractions S_n, M_{nx}, M_{ny}

$$Q_x = -D\frac{\partial}{\partial x}\nabla^2 w, \qquad Q_y = -D\frac{\partial}{\partial y}\nabla^2 w, \tag{4a,b}$$

$$M_x = -D\left(\frac{\partial^2 w}{\partial x^2} + \nu\frac{\partial^2 w}{\partial y^2}\right), \qquad M_y = -D\left(\frac{\partial^2 w}{\partial y^2} + \nu\frac{\partial^2 w}{\partial x^2}\right), \tag{4c,d}$$

$$M_{xy} = -D(1-\nu)\frac{\partial^2 w}{\partial x \partial y} \tag{4e}$$

and n_x, n_y are components of the unit vector of the element external normal to element boundary. In matrix form these vectors may simple be written as

$$\mathbf{v} = \overset{\circ}{\mathbf{v}} + \mathbf{N}\mathbf{c} \quad \text{and} \quad \mathbf{t} = \overset{\circ}{\mathbf{t}} + \mathbf{M}\mathbf{c}, \tag{5a,b}$$

where $\overset{\circ}{\mathbf{v}}$, $\overset{\circ}{\mathbf{t}}$ and $\mathbf{N}$, $\mathbf{M}$ correspond respectively to the particular and homogeneous parts, $\overset{\circ}{w}$ and $\mathbf{W}$, of the internal field (1).

In the considered hybrid approach the elements are linked through an auxiliary displacement frame

$$\tilde{\mathbf{v}} = \begin{Bmatrix} \tilde{w} \\ \tilde{w}_x \\ \tilde{w}_y \end{Bmatrix} = \tilde{\mathbf{N}}\mathbf{d} \tag{6}$$

defined at Γ^e, independently of $\mathbf{v} = \overset{\circ}{\mathbf{v}} + \mathbf{N}\mathbf{c}$, in terms of nodal parameters $\mathbf{d}$, which are final unknowns of the problem, while $\tilde{\mathbf{N}}$ stands for the matrix of known interpolation functions the type of which (Subsection 2.3) depends on the number of DOF chosen at corner nodes (Fig. 1).

The standard force–displacement relationship is assumed in the form

$$\mathbf{r} = \overset{\circ}{\mathbf{r}} + \mathbf{k}\,\mathbf{d}\,, \tag{7}$$

where $\mathbf{r}$ stands for the vector of generalized nodal forces conjugate to $\mathbf{d}$, $\overset{\circ}{\mathbf{r}}$ is the part of $\mathbf{r}$ due to the load p and/or the boundary tractions imposed on Γ^e and $\mathbf{k}$ is a symmetric positive definite stiffness matrix. To obtain this relationship, we first enforce, in a weak sense, conformity on $w = \overset{\circ}{w} + \mathbf{W}\mathbf{c}$,

$$\int_{\Gamma^e} \delta\mathbf{t}^{\mathrm{T}}\,(\mathbf{v} - \tilde{\mathbf{v}})\,\mathrm{d}\Gamma = 0 \tag{8a}$$

(where $\delta\mathbf{t} = \mathbf{M}\delta\mathbf{c}$) and then use the equivalence of virtual works

$$\int_{\Gamma^e} \delta\tilde{\mathbf{v}}^{\mathrm{T}}\mathbf{t}\,\mathrm{d}\Gamma = \delta\mathbf{d}^{\mathrm{T}}\mathbf{r} + \int_{\Gamma_t^e} \delta\tilde{\mathbf{v}}^{\mathrm{T}}\bar{\mathbf{t}}\,\mathrm{d}\Gamma \tag{8b}$$

(where $\bar{\mathbf{t}}$ stands for imposed boundary tractions at the part Γ_t^e of the boundary Γ^e). This makes it possible to eliminate the internal parameters $\mathbf{c}$ in (1)

$$\mathbf{c} = -\mathbf{H}^{-1}\mathbf{g} + \mathbf{H}^{-1}\mathbf{G}\,\mathbf{d} \tag{9}$$

and to evaluate the element matrices $\overset{\circ}{\mathbf{r}}$ and $\mathbf{k}$ in (7) as

$$\overset{\circ}{\mathbf{r}} = \mathbf{h} - \mathbf{G}^{\mathrm{T}}\mathbf{H}^{-1}\mathbf{g} \qquad \text{and} \qquad \mathbf{k} = \mathbf{G}^{\mathrm{T}}\mathbf{H}^{-1}\mathbf{G} \tag{10a,b}$$

The auxiliary matrix quantities in (9) and (10a,b) are obtained from the following boundary integrals:

$$\mathbf{G} = \int_{\Gamma^e} \mathbf{M}^{\mathrm{T}}\tilde{\mathbf{N}}\,\mathrm{d}\Gamma\,, \qquad \mathbf{H} = \int_{\Gamma^e} \mathbf{M}^{\mathrm{T}}\mathbf{N}\,\mathrm{d}\Gamma = \int_{\Gamma^e} \mathbf{N}^{\mathrm{T}}\mathbf{M}\,\mathrm{d}\Gamma\,, \tag{11a,b}$$

$$\mathbf{g} = \int_{\Gamma^e} \mathbf{M}^{\mathrm{T}}\,\overset{\circ}{\mathbf{v}}\,\mathrm{d}\Gamma\,, \qquad \mathbf{h} = \int_{\Gamma^e} \tilde{\mathbf{N}}^{\mathrm{T}}\,\overset{\circ}{\mathbf{t}}\,\mathrm{d}\Gamma - \int_{\Gamma_t^e} \tilde{\mathbf{N}}^{\mathrm{T}}\bar{\mathbf{t}}\,\mathrm{d}\Gamma\,. \tag{11c,d}$$

The symmetry of $\mathbf{H}$ is obvious if one observes that in the absence of distributed load p and, as a consequence, with vanishing $\overset{\circ}{\mathbf{v}}$ and $\overset{\circ}{\mathbf{t}}$, the strain energy may be evaluated from Clapeyron's theorem as

$$\begin{aligned} U &= \frac{1}{2}\int_{\Gamma^e} \mathbf{t}^{\mathrm{T}}\mathbf{v}\,\mathrm{d}\Gamma = \frac{1}{2}\int_{\Gamma^e} \mathbf{v}^{\mathrm{T}}\mathbf{t}\,\mathrm{d}\Gamma \\ &= \frac{1}{2}\mathbf{c}^{\mathrm{T}}\int_{\Gamma^e} \mathbf{M}^{\mathrm{T}}\mathbf{N}\,\mathrm{d}\Gamma\,\mathbf{c} = \frac{1}{2}\mathbf{c}^{\mathrm{T}}\int_{\Gamma^e} \mathbf{N}^{\mathrm{T}}\mathbf{M}\,\mathrm{d}\Gamma\,\mathbf{c} = \frac{1}{2}\mathbf{c}^{\mathrm{T}}\mathbf{H}\,\mathbf{c}\,. \end{aligned} \tag{12}$$

This also implies that $\mathbf{k}$, as defined by (10b), is a symmetric positive definite matrix.

It is interesting to observe that the relations (9) to (11) may also be obtained from a simple variational formulation stated as [20]

$$H(w, \tilde{w}) = \Pi(\tilde{w}) - \sum_e U^e(\varepsilon - \tilde{\varepsilon}) = \text{stationary}\,, \tag{13}$$

where $\Pi(\tilde{w})$ is the total potential energy written in terms of the C^1 conforming displacements $\tilde{w}$, $U^e(\varepsilon - \tilde{\varepsilon})$ stands for strain energy of the difference between the generalized strains

$$\varepsilon = \left\{ -\frac{\partial^2 w}{\partial x^2} \quad -\frac{\partial^2 w}{\partial y^2} \quad -2\frac{\partial^2 w}{\partial x \partial y} \right\}^{\mathrm{T}} \quad \text{and} \quad \tilde{\varepsilon} = \left\{ -\frac{\partial^2 \tilde{w}}{\partial x^2} \quad -\frac{\partial^2 \tilde{w}}{\partial y^2} \quad -2\frac{\partial^2 \tilde{w}}{\partial x \partial y} \right\}^{\mathrm{T}} \tag{13a,b}$$

and the sum $\sum_e$ extends over all elements. Here, formally, the conforming field $\tilde{w}$ extends over whole subdomain Ω^e of each element but, after the variation of H, all domain integrals in $\delta H = 0$ may be replaced (by virtue of Clapeyron's principle) by equivalent boundary integrals. As a consequence, instead of $\tilde{w}$ on Ω^e one finally needs to know explicitly only the corresponding $\tilde{\mathbf{v}}$ on Γ^e.

2.2. Internal displacement field w of the element

As a rule, the homogeneous part of the displacement field in (1) is obtained by suitably truncating a T-complete set (following the terminology proposed by Zieliński and Zienkiewicz [21]) of regular homogeneous solutions W_j. This feature relates the HT elements to the non-conventional boundary methods studied by Herrera and coworkers [22]. In the present case, the most suitable choice of such a set are biharmonic polynomials which may be generated in a systematic way by taking in turn the real and the imaginary parts of two complex functions, $(r/d)^2 (z/d)^k$ and $(z/d)^{k+2}$, namely

$$\left.\begin{aligned} W_j &= \left(\frac{r}{d}\right)^2 \operatorname{Im}\left(\frac{z}{d}\right)^k \qquad & W_{j+1} &= \left(\frac{r}{d}\right)^2 \operatorname{Re}\left(\frac{z}{d}\right)^k \\ W_{j+2} &= \operatorname{Im}\left(\frac{z}{d}\right)^{k+2} \qquad & W_{j+3} &= \operatorname{Re}\left(\frac{z}{d}\right)^{k+2} \\ & & k &= 0, 1, 2, \ldots \end{aligned}\right\}, \tag{14}$$

where

$$r^2 = x^2 + y^2, \qquad z = x + \mathrm{i}y, \tag{14a,b}$$

x, y are Cartesian coordinates originated at the element centroid (Fig. 1) and d is taken as the average distance between the element centroid and element corners. As for $k = 0$ $W_j = W_0 = 0$, the generating sequence (14) starts with $W_{j+1} = W_1$. The reason for using the local coordinates and dividing them by d is to preserve the desirable invariant properties under translation of the global coordinates X and Y and to avoid numerical problems (overflow or underflow) arising for high values of the exponent k.

The load dependent term $\overset{\circ}{w}$ in (1) may easily be found for various types of continuous or discontinuous loads (line loads, patch loads, ...) as well as the singular concentrated load (see [7, 10, 11, 13]). Here will be given only those of them which will be considered in the subsequent numerical studies (Section 3), namely

$$\overset{\circ}{w} = \frac{pr^4}{64D} \qquad \text{for uniform load } p = \text{const} \tag{15}$$

and

$$\overset{\circ}{w} = \frac{P}{16\pi D} r_P^2 \ln r_P^2 \qquad \text{for concentrated load } P \text{ at } X_P, Y_P, \tag{16}$$

where

$$r_P^2 = (X - X_P)^2 + (Y - Y_P)^2 . \tag{16a}$$

To take full advantage of the HT approach (possibility of arbitrary located P without need of mesh adjustments), the term (16) should be used as a global function extending over all elements, or as a semi-global one, confined by the program automatically to a patch of elements situated in the neighbourhood of P — see [23]. Though correct from a mathematical point of view, the singular solution (16) however violates the basic assumptions of the theory of small deformations since for $r \to r_P$ the generalized deformations (and hence the moments) go to infinity. Therefore a more realistic approach consists in assuming that P is uniformly distributed over a small circular area of optional radius b, in which case [7], with $\rho = r_P/d$ and $\beta = b/d$

for $\rho \leq \beta$

$$\overset{\circ}{w} = \left[\frac{\beta^2}{64}(4\ln\beta - 3) + \frac{1}{16} + \frac{\rho^2}{32}\left(4\ln\beta - \beta^2\right) + \frac{\rho^4}{64\beta^2}\right]\frac{Pd^2}{\pi D} \tag{17a}$$

for $\rho \geq \beta$

$$\overset{\circ}{w} = \left[\frac{1}{32}\left(2 + \beta^2\right)\left(1 - \rho^2\right) + \frac{1}{16}\left(\beta^2 + 2\rho^2\right)\ln\rho\right]\frac{Pd^2}{\pi D} \tag{17b}$$

2.3. Alternative formulations of displacement frame

Unlike the conventional conforming assumed displacement thin plate p-elements (thus far confined to triangular elements [24]), the generation of HT p-elements for C^1 conformity problems does not present any particular difficulty. Since no area integrals are involved, the HT p-element may have an arbitrary number of sides. The components of the displacement frame vector (6) may conveniently be expressed in terms of two functions, $\tilde{w}$ (displacement) and $\tilde{\varphi} = \tilde{w}_n$ (normal slope), namely

$$\tilde{v} = \begin{Bmatrix} \tilde{w} \\ \tilde{w}_x \\ \tilde{w}_y \end{Bmatrix} = \begin{Bmatrix} \tilde{w} \\ \bar{n}_x\tilde{\varphi} - \bar{n}_y \partial\tilde{w}/\partial s \\ \bar{n}_y\tilde{\varphi} + \bar{n}_x \partial\tilde{w}/\partial s \end{Bmatrix}, \tag{18}$$

where

$$\partial/\partial s = -\bar{n}_y \partial/\partial x + \bar{n}_x \partial/\partial y \tag{18a}$$

and where for a particular boundary segment $A - C - B$ (Fig. 1) of length $l_{AB} = 2a$

$$\bar{n}_x = \frac{1}{l_{AB}}(y_B - y_A), \qquad \bar{n}_y = -\frac{1}{l_{AB}}(x_B - x_A). \tag{18b,c}$$

If the segment $A - C - B$ belongs to the interelement boundary, common to two neighbouring elements, then $\bar{n}_x$ and $\bar{n}_y$ are equal to the components n_x and n_y of the unit vector of external normal of the one of the two elements along the boundary of which the sequence $A - C - B$ defines the anticlockwise rotation (Fig. 1). They are equal to $-n_x$ and $-n_y$ for the element where the sequence $A - C - B$ corresponds to the opposite sense of rotation.

Three alternative displacement formulations presenting respectively 1, 3 and 6 DOF at corner nodes ○ along with an optional number, M, of DOF alloted to fictitious mid-side nodes △ will be studied. Hereafter a particular element side $A - C - B$ (Fig. 1) will be considered and appropriate definitions of the subvectors $\mathbf{d}_A$, $\mathbf{d}_B$, $\mathbf{d}_C$ of the vector $\mathbf{d}$ and of the functions $\tilde{w}$ and $\tilde{\varphi}$ be given.

2.3.1. Frame with 1 DOF at corner nodes (Fig. 3)

Here

$$\mathbf{d}_A = \{\tilde{w}_A\}, \qquad \mathbf{d}_B = \{\tilde{w}_B\} \tag{19a,b}$$

and

$$\mathbf{d}_C = \left\{ {}^1\Delta\tilde{\varphi}_C \;\; {}^1\Delta\tilde{w}_C \;\; {}^2\Delta\tilde{\varphi}_C \;\; {}^2\Delta\tilde{w}_C \;\; \ldots \;\; \text{etc.} \right\}^{\mathrm{T}}, \tag{19c}$$

where the parameters ${}^1\Delta\tilde{\varphi}_C$, ${}^1\Delta\tilde{w}_C$, ${}^2\Delta\tilde{\varphi}_C$, ${}^2\Delta\tilde{w}_C, \ldots$, etc. associated for convenience with the mid-side node C, correspond to hierarchic side-modes displayed in Fig. 3. With the shape functions $\tilde{N}_i$ *in this figure, the frame functions $\tilde{w}$ and $\tilde{\varphi}$ are equal to*

$$\begin{aligned} \tilde{w} &= \tilde{N}_1\tilde{w}_A + \tilde{N}_2\tilde{w}_B + \tilde{N}_3\,{}^1\Delta\tilde{w}_C + \tilde{N}_5\,{}^2\Delta\tilde{w}_C + \ldots \\ &= \tilde{N}_1\tilde{w}_A + \tilde{N}_2\tilde{w}_B + \sum_{k=1,2,\ldots} \tilde{N}_{2k+1}\,{}^k\Delta\tilde{w}_C \end{aligned} \tag{20a}$$

$$\tilde{\varphi} = \tilde{N}_4\,{}^1\Delta\tilde{\varphi}_C + \tilde{N}_6\,{}^2\Delta\tilde{\varphi}_C + \ldots = \sum_{k=1,2,\ldots} \tilde{N}_{2k+2}\,{}^k\Delta\tilde{\varphi}_C \tag{20b}$$

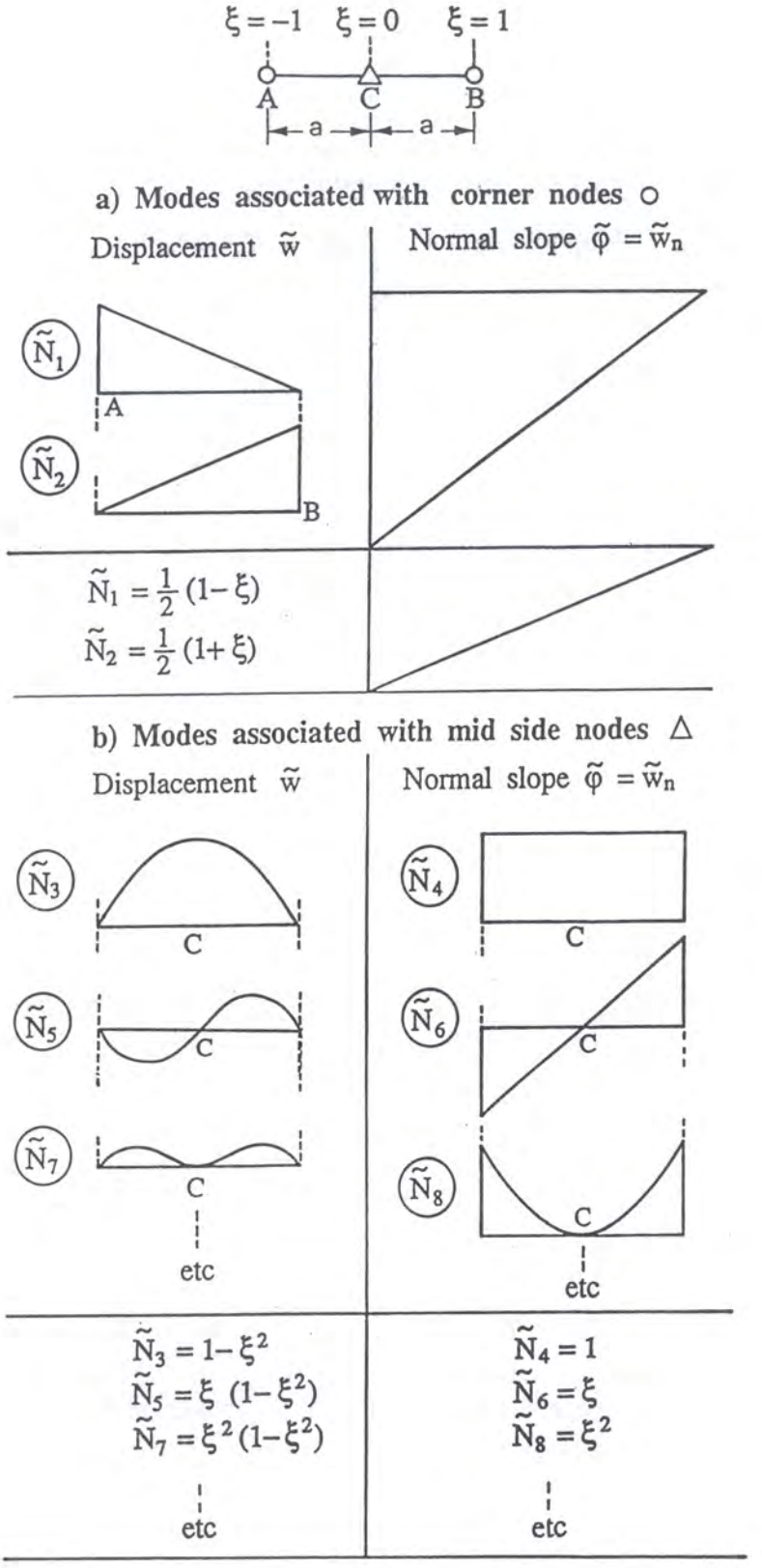

Fig. 3. Frame functions of HT thin plate *p*-element with single DOF at element corners

2.3.2. Frame with 3 DOF at corner nodes (Fig. 4)

In this case

$$\mathbf{d}_A = \{\tilde{w}_A \;\; \tilde{w}_{xA} \;\; \tilde{w}_{yA}\}^{\mathrm{T}}, \qquad \mathbf{d}_B = \{\tilde{w}_B \;\; \tilde{w}_{xB} \;\; \tilde{w}_{yB}\}^{\mathrm{T}} \tag{21a,b}$$

and $\mathbf{d}_C$ is defined by the relation (19c). With the shape functions from Fig. 4, $\tilde{w}$ and $\tilde{\varphi}$ along the side $A-C-B$ of the element have now the following definitions:

$$\begin{aligned}\tilde{w} &= \tilde{N}_1\tilde{w}_A + \tilde{N}_2\tilde{w}_{\xi A} + \tilde{N}_3\tilde{w}_B + \tilde{N}_4\tilde{w}_{\xi B} + \tilde{N}_7{}^1\Delta\tilde{w}_C + \tilde{N}_9{}^2\Delta\tilde{w}_C + \ldots \\ &= \tilde{N}_1\tilde{w}_A + \tilde{N}_2\tilde{w}_{\xi A} + \tilde{N}_3\tilde{w}_B + \tilde{N}_4\tilde{w}_{\xi B} + \sum_{k=1,2,\ldots} \tilde{N}_{2k+5}{}^k\Delta\tilde{w}_C\,,\end{aligned} \tag{22a}$$

$$\begin{aligned}\tilde{\varphi} &= \tilde{N}_5\tilde{\varphi}_A + \tilde{N}_6\tilde{\varphi}_B + \tilde{N}_8{}^1\Delta\tilde{\varphi}_C + \tilde{N}_{10}{}^2\Delta\tilde{\varphi}_C + \ldots \\ &= \tilde{N}_5\tilde{\varphi}_A + \tilde{N}_6\tilde{\varphi}_B + \sum_{k=1,2,\ldots} \tilde{N}_{2k+6}{}^k\Delta\tilde{\varphi}_C\,.\end{aligned} \tag{22b}$$

In the first of these equations, the parameters $\tilde{w}_{\xi A}$ and $\tilde{w}_{\xi B}$ stand for the first derivatives of $\tilde{w}$ at the ends A and B of the segment with respect to the non-dimensional coordinate ξ varying from -1 to $+1$ between A and B. These 'local' parameters, as well as the 'local' parameters $\tilde{\varphi}_A$ and $\tilde{\varphi}_B$ in the second equation, may be expressed as follows in terms of the 'global' parameters $\tilde{w}_{xA}$, $\tilde{w}_{yA}$ and $\tilde{w}_{xB}$, $\tilde{w}_{yB}$:

$$\tilde{w}_{\xi A} = -a\,(\bar{n}_y\tilde{w}_{xA} - \bar{n}_x\tilde{w}_{yA})\,, \tag{23a}$$

$$\tilde{w}_{\xi B} = -a\,(\bar{n}_y\tilde{w}_{yB} - \bar{n}_x\tilde{w}_{yB}) \tag{23b}$$

and

$$\tilde{\varphi}_A = \bar{n}_x\tilde{w}_{xA} + \bar{n}_y\tilde{w}_{yA}\,, \tag{23c}$$

$$\tilde{\varphi}_B = \bar{n}_x\tilde{w}_{xB} + \bar{n}_y\tilde{w}_{yB}\,. \tag{23d}$$

Above, a stands for half of the length of the element side (see Fig. 4).

2.3.3. Frame with 6 DOF at corner nodes (Fig. 5)

Here the subvectors of nodal parameters at corner nodes have the following definition

$$\mathbf{d}_A = \{\tilde{w}_A \;\; \tilde{w}_{xA} \;\; \tilde{w}_{yA} \;\; \tilde{w}_{xxA} \;\; \tilde{w}_{xyA} \;\; \tilde{w}_{yyA}\}^{\mathrm{T}}\,, \tag{24a}$$

$$\mathbf{d}_B = \{\tilde{w}_B \;\; \tilde{w}_{xB} \;\; \tilde{w}_{yB} \;\; \tilde{w}_{xxB} \;\; \tilde{w}_{xyB} \;\; \tilde{w}_{yyB}\}^{\mathrm{T}}\,. \tag{24b}$$

As in the preceding formulations, for the subvector $\mathbf{d}_C$ at the mid-side node C holds true the definition (19c). With the shape functions from Fig. 5, the deflection $\tilde{w}$ and the normal rotation $\tilde{\varphi}$ along $A-C-B$ may now be written as follows:

$$\begin{aligned}\tilde{w} &= \tilde{N}_1\tilde{w}_A + \tilde{N}_2\tilde{w}_{\xi A} + \tilde{N}_3\tilde{w}_{\xi\xi A} \\ &\quad + \tilde{N}_4\tilde{w}_B + \tilde{N}_5\tilde{w}_{\xi B} + \tilde{N}_6\tilde{w}_{\xi\xi B} + \sum_{k=1,2,\ldots} \tilde{N}_{2k+9}{}^k\Delta\tilde{w}_C\,,\end{aligned} \tag{25a}$$

$$\tilde{\varphi} = \tilde{N}_7\tilde{\varphi}_A + \tilde{N}_8\tilde{\varphi}_{\xi A} + \tilde{N}_9\tilde{\varphi}_B + \tilde{N}_{10}\tilde{\varphi}_{\xi B} + \sum_{k=1,2,\ldots} \tilde{N}_{2k+10}{}^k\Delta\tilde{\varphi}_C\,. \tag{25b}$$

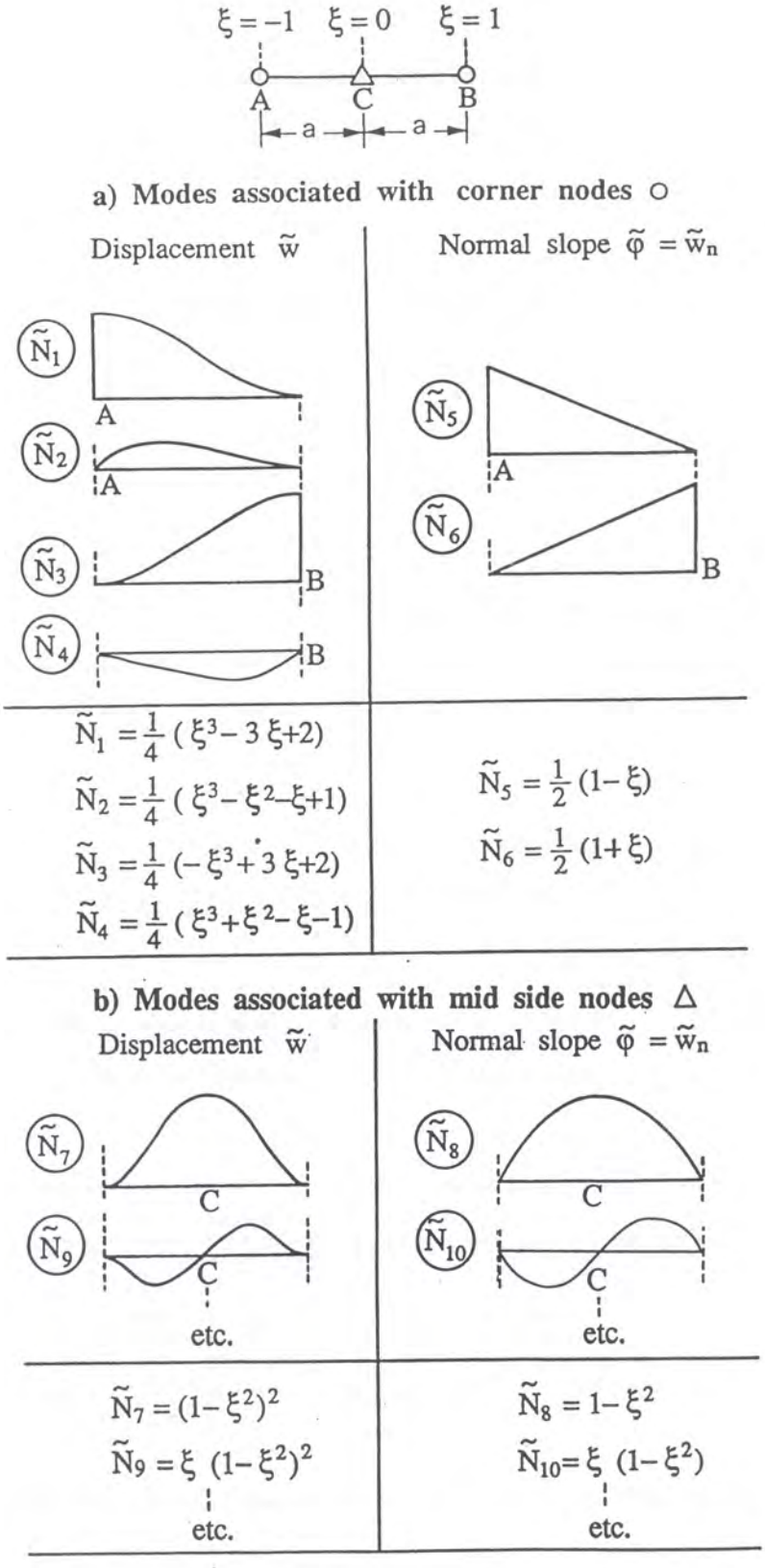

Fig. 4. Frame functions of HT thin plate *p*-element with 3 DOF at element corners

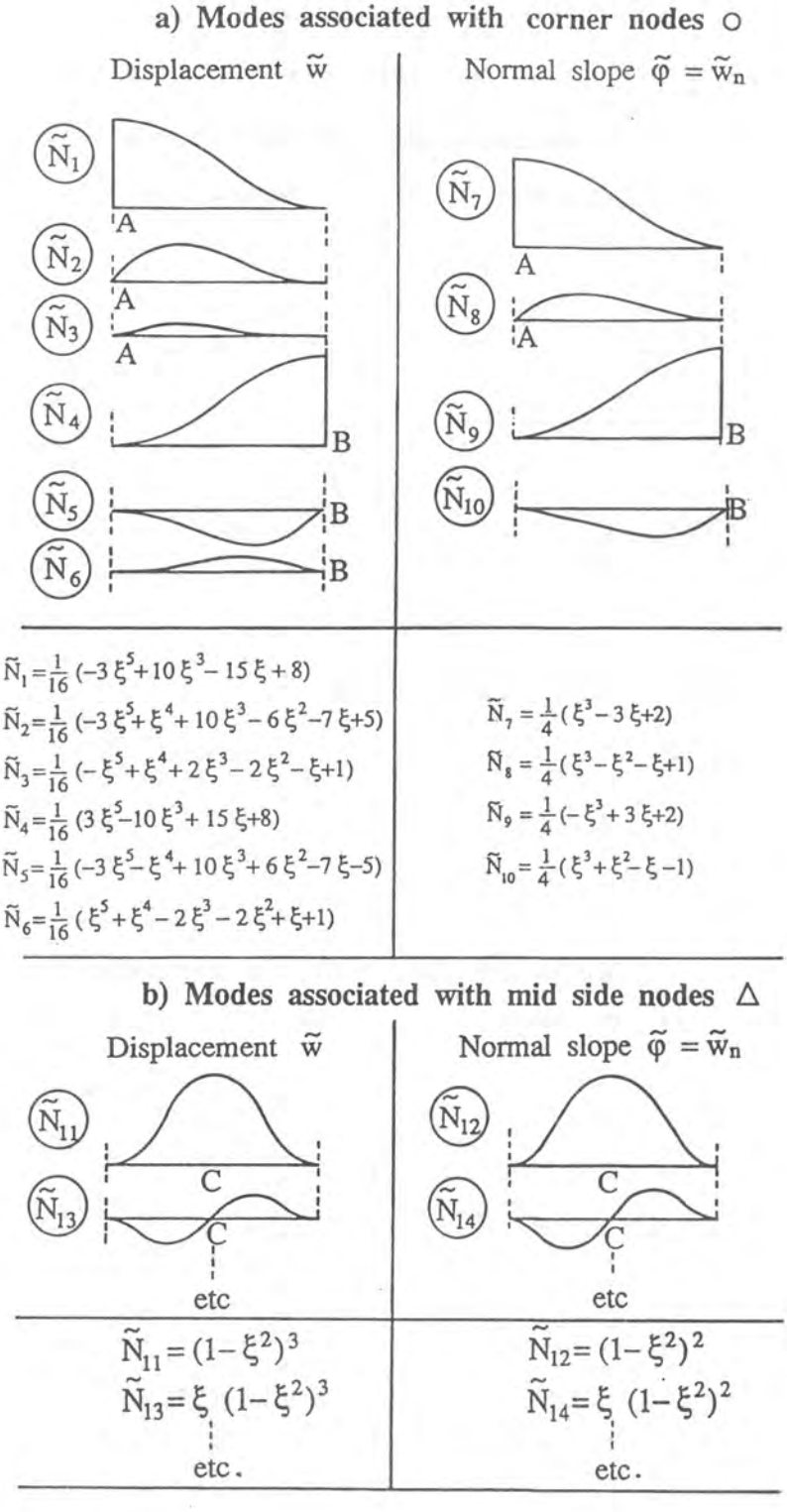

Fig. 5. Frame functions of HT thin plate p-element with 6 DOF at element corners

As in paragraph 2.3.2, the 'local' parameters $\tilde{w}_{\xi A}$, $\tilde{w}_{\xi B}$ and $\tilde{\varphi}_A$, $\tilde{\varphi}_B$ may again be expressed in terms of $\tilde{w}_{xA}$, $\tilde{w}_{yA}$, $\tilde{w}_{xB}$, $\tilde{w}_{yB}$ by the transformation (23a–d). Moreover, for the higher order 'local' parameters, $\tilde{w}_{\xi\xi A}$, $\tilde{w}_{\xi\xi B}$ and $\tilde{\varphi}_{\xi A}$, $\tilde{\varphi}_{\xi B}$ apply the following relations:

$$\tilde{w}_{\xi\xi A} = a^2 \left(\bar{n}_y^2 \tilde{w}_{xxA} - \bar{n}_x \bar{n}_y \tilde{w}_{xyA} + \bar{n}_x^2 \tilde{w}_{yyA} \right) , \tag{26a}$$

$$\tilde{w}_{\xi\xi B} = a^2 \left(\bar{n}_y^2 \tilde{w}_{xxB} - \bar{n}_x \bar{n}_y \tilde{w}_{xyB} + \bar{n}_x^2 \tilde{w}_{yyB} \right) \tag{26b}$$

and

$$\tilde{\varphi}_{\xi A} = -a \left[\bar{n}_x \bar{n}_y \tilde{w}_{xxA} - \left(\bar{n}_x^2 - \bar{n}_y^2 \right) \tilde{w}_{xyA} - \bar{n}_x \bar{n}_y \tilde{w}_{yyA} \right] , \tag{26c}$$

$$\tilde{\varphi}_{\xi B} = -a \left[\bar{n}_x \bar{n}_y \tilde{w}_{xxB} - \left(\bar{n}_x^2 - \bar{n}_y^2 \right) \tilde{w}_{xyB} - \bar{n}_x \bar{n}_y \tilde{w}_{yyB} \right] , \tag{26d}$$

where $\bar{n}_x$ and $\bar{n}_y$ are again defined by the relations (18b,c).

2.4. Implementation

Since no area integration is involved, a single element subroutine may be written for a p-element with an optional number of sides and an optional type of the displacement frame. The number m of homogeneous solutions W_j in the internal element field (1) will be adjusted automatically in terms of the total number n of DOF of the displacement frame of the element. The necessary (but not sufficient) condition for the element stiffness matrix to have the correct rank is stated as [7, 8]

$$m \geq n - m_{\mathrm{RIG}} = n - 3 , \tag{27}$$

where m_{RIG} stands for the number of rigid body modes. Though the use of the minimal $m = n - 3$ does not always guarantee a stiffness matrix with the full rank of $(n - 3)$, full rank may always be achieved by suitably augmenting m. As $\mathrm{Im}(z/a)^0 = 0$, the generating sequence (14) yields for $k = 0$ only three non vanishing homogeneous solutions and, as a consequence, with $k > 0$ one obtains $4k + 3$ homogeneous solutions.

The numerical studies in Section 3 will be confined to quadrilateral elements in which case with $N = 1, 3$ or 6 DOF at corner nodes and $M = 1, 3, 5, \ldots$ etc. hierarchical DOF at mid-side nodes, the element will present a $n \times n$ stiffness matrix with n equal to

$$n = 4 \, (N + M) . \tag{28}$$

It is of interest to observe that the side-mode hierarchical DOF in $\mathbf{d}_C$ (see (19c)) are ranged so that the polynomial degree of the frame is alternatively increased for the normal slope $\tilde{\varphi}$ and the transversal displacement $\tilde{w}$. Moreover, the reason for starting with improving $\tilde{\varphi}$ ($M = 1$) and then upgrading M by steps of two is to keep the polynomial degree of $\tilde{\varphi}$ one degree lower than that ($\tilde{p}$) of the displacement $\tilde{w}$.

The standard eigenvalues tests have shown that while for quadrilateral HT p-elements with 1 or 3 DOF at element corners the minimum number of homogeneous solutions W_i, namely

$$m = n - 3 \quad \text{if} \quad N = 1 \text{ or } 3 \tag{29a}$$

warrants a stiffness matrix with full rank, in the case of 6 DOF at element corners two additional homogeneous solutions are necessary,

$$m = n - 1 \quad \text{if} \quad N = 6 \tag{29b}$$

to ensure the $\mathbf{k}$ matrix with full rank. Indeed, with $m = n - 3$, the element stiffness matrix may present a spurious zero energy mode.

One of the most desirable features of the implementation are the invariant properties of the element under the rotation of the coordinate axes. The use of the complex form (14) makes it easy to understand that such properties will be preserved if care is taken to truncate the generating sequence (14) either after the two biharmonic functions, $(r/d)^2\mathrm{Im}(\dot{z}/d)^k$ and $(r/d)^2\mathrm{Re}(z/d)^k$, or after the two harmonic functions, namely $\mathrm{Im}(z/d)^{k+2}$ and $\mathrm{Re}(z/d)^{k+2}$. Since for $k = 0$ there are only three independent solutions, the total number, m, of homogeneous solution in (1) has to be odd. Note also that the expressions (15) to (17) of the particular part of the solution have been chosen so as to be invariant if the coordinate axes are turned.

In order to ensure that the orientation of the non-dimensional coordinate ξ (Fig. 3 to 5) will be the same for the interelement portion of the boundary between two elements, the simplest method consists in choosing the nodes A ($\xi_A = -1$) and B ($\xi_B = 1$) so that the corresponding global numbers N_{OA} and N_{OB} of these nodes in the FE mesh fulfil the condition:

$$N_{OA} < N_{OB}\,. \tag{30}$$

As may be seen from the generating sequence (14), the internal displacement field is in error by rigid body modes. Indeed the inclusion of such modes would render the hybrid matrix $\mathbf{H}$ (11b) singular for inversion [7]. However, once the element assembly has been solved for nodal displacements, then in each element the three missing rigid body modes, namely

$$c_{R0}, \quad c_{R1}x \quad \text{and} \quad c_{R2}y\,, \tag{31}$$

where c_{R0}, c_{R1}, c_{R2} stand for undetermined coefficients, can easily be recovered. In the present paper these coefficients were obtained by a simple procedure based on a least squares matching between the frame function $\tilde{w}$ and the augmented internal field (relation (1) plus the terms (31)) of the element.

3. Assessment

3.1. Preliminary remarks

Most of the numerical studies presented in this section refer to the conventionally used square plate test with undistorted and distorted FE meshes and to the well known Morley's 30° rhombic plate. Unless stated otherwise, the information concerning the mesh density concern the whole domain rather than a symmetric quadrant. Furthermore, a Poisson's ratio $\nu = 0.3$ has been used in all examples.

Though the theoretical formulation from Section 2 allows for p-elements with any number of sides, the present study is confined to quadrilateral elements. An overview of parameters characterising the three p-elements families with 1, 3, 6 DOF at corner nodes is displayed on Table 1. The polynomial degree of the frame function $\tilde{\varphi}$ is always one degree lower as that ($\tilde{p}$) of the frame function $\tilde{w}$.

3.2. Simply supported square plate

3.2.1. Comparison of accuracy in nodal averages

The aim of this study was to analyze the influence of the number of DOF at corner nodes on the accuracy and the performance of the p-extension process. A uniform 2×2 FE mesh (Fig. 6a) over the whole plate was used and the number M of side-mode DOF was varied. Table 2 displays some results obtained for uniform load at points A, B and C (Fig. 6) of the plate. In addition to the central deflection w_C and central moment $M_{xC} = M_{yC}$, the predicted shear force Q_{yB} and corner reaction $V_A = 2M_{xyA}$ are also indicated. The exact results given in the last column of the table

Table 1. Control parameters characterising three families of quadrilateral HT elements with 1, 3, 6 DOF at corner nodes and optional number of side-modes DOF. M and $\bar{p}$: number of side-modes DOF and corresponding polynomial degree of frame function $\tilde{w}$; m and p: number of Trefftz functions in (1) and corresponding degree of internal field w

Quantity	N	n — number of element's DOF								
		16	24	28	32	36	40	44	48	52
M	1	3	5	–	7	–	9	–	11	–
	3	1	3	–	5	–	7	–	9	–
	6	–	–	1	–	3	–	5	–	7
$\bar{p}$	1	2	3	–	4	–	5	–	6	–
	3	3	4	–	5	–	6	–	7	–
	6	–	–	5	–	6	–	7	–	8
m	1	13	21	–	29	–	37	–	45	–
	3	13	21	–	29	–	37	–	45	–
	6	–	–	27	–	35	–	43	–	51
p	1	5	7	–	9	–	11	–	13	–
	3	5	7	–	9	–	11	–	13	–
	6	–	–	8	–	10	–	12	–	14

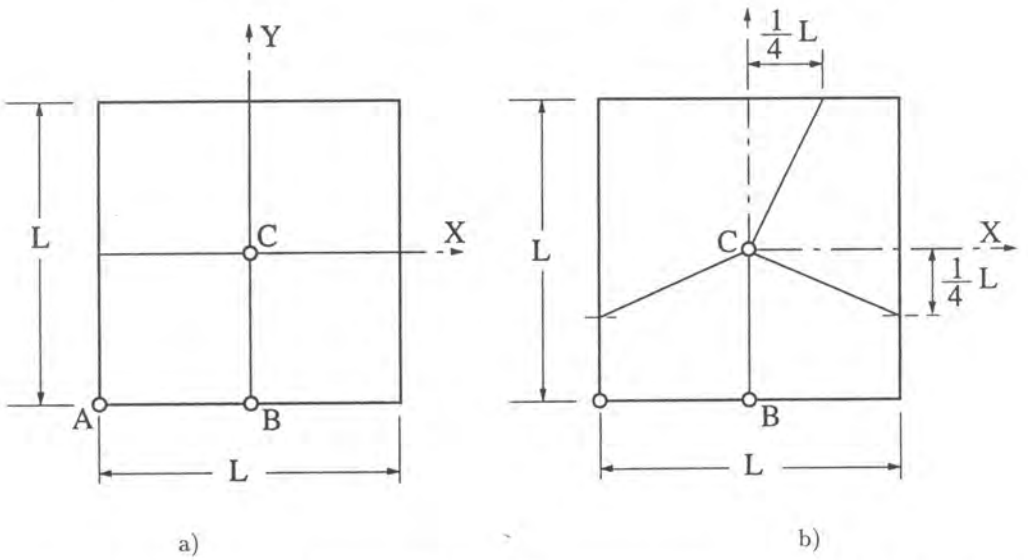

Fig. 6. Undistorted (a) and distorted (b) 2 × 2 HT element meshes over square plate of side L

were obtained from the converged double series Navier solution [25]. The percentage errors of the FE results from Table 2 are displayed on Table 3. These errors are defined as

$$\Delta f\,\% = \frac{f_{\mathrm{FE}} - f_{\mathrm{EX}}}{f_{\mathrm{EX}}} \times 100\,, \tag{32}$$

where f_{FE} stands for the FE results and f_{EX} for the exact solution.

In the case of elements with 6 DOF at corners, the second row of results corresponds to an alternative specification of boundary conditions at element corner nodes. Here the higher order DOF, $\tilde{w}_{xx}$ and $\tilde{w}_{yy}$, have made it possible to strongly impose the natural condition $M_n = 0$ by simply setting $\tilde{w}_{nn} = 0$.

The inspection of percentage errors shown on Table 3 calls for two comments. The first concerns the excellent accuracy of the predicted shear force and corner reaction, impossible to achieve with conventional p-elements. The second concerns the effect of the number of DOF at corner nodes, which appears to be smaller in this example than was expected. Indeed, though for a given size of

Table 2. Results of p-extension process with uniform 2×2 HT-element mesh (Fig.6a) over simply supported uniformly loaded plate

Quantity	N (DOF at el. corners)	Number of lines and columns of element stiffness matrix									Exact
		16	24	28	32	36	40	44	48	52	
$\frac{10^2 D w_C}{pL^4}$	1	0.406946	0.405862	—	0.406317	—	0.406234	—	0.406237	—	0.406235
	3	0.408745	0.405839	—	0.406243	—	0.406234	—	0.406235	—	
	6	—	—	0.406259	—	0.406234	—	0.406235	—	0.406235	
	6[1)]	—	—	0.406263	—	0.406234	—	0.406234	—	0.406235	
$\frac{10 M_{xC}}{pL^2}$	1	0.579609	0.489455	—	0.479225	—	0.480081	—	0.479200	—	0.478864
	3	0.518191	0.481536	—	0.479306	—	0.478984	—	0.478892	—	
	6	—	—	0.480286	—	0.479317	—	0.479038	—	0.478944	
	6[1)]	—	—	0.480562	—	0.479270	—	0.479024	—	0.478944	
$\frac{Q_{yB}}{pL}$	1	0.322817	0.329891	—	0.333589	—	0.336082	—	0.337786	—	0.337657
	3	0.283991	0.340545	—	0.334659	—	0.339033	—	0.336802	—	
	6	—	—	0.335802	—	0.338348	—	0.337340	—	0.337797	
	6[1)]	—	—	0.337457	—	0.338973	—	0.336947	—	0.337849	
$\frac{10 V_A}{pL^2}$	1	0.661945	0.680647	—	0.654597	—	0.651680	—	0.649883	—	0.649662
	3	0.679830	0.658191	—	0.651282	—	0.650565	—	0.650158	—	
	6	—	—	0.647317	—	0.649121	—	0.649616	—	0.649716	
	6[1)]	—	—	0.647122	—	0.649156	—	0.649627	—	0.649717	

[1)] With $\tilde{w}_{nn} = 0$ imposed at plate boundary nodes

Table 3. Percentage errors in predicted FE results from Table 2 (Uniform 2 × 2 HT p-element mesh over simply supported uniformly loaded square plate

Quantity	N (DOF at el. corners)	Number of lines and columns of element stiffness matrix								
		16	24	28	32	36	40	44	48	52
Δw_C %	1	0.17	-0.09	—	0.02	—	0.00	—	0.00	—
	3	0.62	-0.10	—	0.00	—	0.00	—	0.00	—
	6	—	—	0.01	—	0.00	—	0.00	—	0.00
	6[1)]	—	—	0.01	—	0.00	—	0.00	—	0.00
ΔM_{xC} %	1	21.04	2.21	—	0.07	—	0.25	—	0.07	—
	3	8.21	0.56	—	0.09	—	0.03	—	0.01	—
	6	—	—	0.30	—	0.09	—	0.04	—	0.02
	6[1)]	—	—	0.35	—	0.08	—	0.03	—	0.02
ΔQ_{yB} %	1	-4.40	-2.30	—	-1.20	—	-0.47	—	0.04	—
	3	-15.89	0.86	—	-0.89	—	0.14	—	-0.25	—
	6	—	—	-0.55	—	0.20	—	-0.09	—	0.04
	6[1)]	—	—	-0.06	—	0.39	—	-0.21	—	0.06
ΔV_A %	1	1.89	4.77	—	0.76	—	0.31	—	0.03	—
	3	4.64	1.31	—	0.25	—	0.14	—	0.08	—
	6	—	—	-0.36	—	-0.08	—	-0.01	—	0.01
	6[1)]	—	—	-0.39	—	-0.08	—	-0.01	—	0.01

[1)] With $\tilde{w}_{nn} = 0$ imposed at plate boundary nodes

the element stiffness matrix the polynomial degree of the frame is lowest for $N = 1$ and largest for $N = 6$ (Table 1), the results appear to be, on average, of comparable quality.

The study of the uniformly loaded plate was completed by that of the centrally loaded one. The concentrated load P was considered either as a nodal load (Tables 4 and 5) or assumed uniformly distributed over a small circular area with radius $b = L/1000$ (Tables 6 and 7) and accounted for by the discontinuous particular solution $\overset{\circ}{w}$ defined by relations (17a,b). The comparison of results clearly shows the superiority of the latter approach over the former one (in particular in the accuracy of the predicted corner reaction V_A).

3.2.2. Accuracy of results derived from the auxiliary frame field

While the results presented thus far have been derived from the internal Trefftz field (1), some results at the element corners may also be obtained from the auxiliary frame field (6). In addition to displacement $\tilde{w}$ (the first nodal parameter) the second order DOF (see (24a,b)) in the case with 6 DOF at corner nodes enable one to perform a particularly simple calculation of bending and twisting moments if use is made of the following relations:

$$\tilde{M}_x = -D\,(\tilde{w}_{xx} + \nu\tilde{w}_{yy})\,, \qquad \tilde{M}_y = -D\,(\tilde{w}_{yy} + \nu\tilde{w}_{xx})\,, \tag{33a,b}$$

$$\tilde{M}_{xy} = -D\,(1-\nu)\,\tilde{w}_{xy}\,. \tag{33c}$$

Some such results and the corresponding percentage errors for the simply supported and uniformly loaded square plate (Fig. 6a) are displayed on Tables 8 and 9. Less accurate than those derived from the internal field (1) (Tables 2 and 3), but obtained at a nearly no cost from the available nodal parameters, these results also render useless the calculation of nodal averages.

The results for uniform load were again completed by those for concentrated central load (Tables 10 and 11). Since previously the results for the concentrated load taken as nodal load were found less accurate (paragraph 3.2.1), only the results obtained by the application of the load term (17a,b) were shown.

Table 4. Centrally loaded simply supported square plate. 2×2 HT p-elements mesh (Fig. 6a) used over whole plate. Central load taken as nodal load

Quantity	N (DOF at el. corners)	Number of lines and columns of element stiffness matrix									Exact
		16	24	28	32	36	40	44	48	52	
$\frac{10Dw_C}{PL^2}$	1	0.128353	0.120348	—	0.117948	—	0.117042	—	0.116648	—	0.1160084
	3	0.111309	0.115109	—	0.115747	—	0.115898	—	0.115969	—	
	6	—	—	0.115688	—	0.115893	—	0.115974	—	0.116003	
	6[1)]	—	—	0.115608	—	0.115856	—	0.115952	—	0.115988	
$\frac{V_A}{P}$	1	0.040028	0.071255	—	0.076547	—	0.082357	—	0.087149	—	0.1219053
	3	0.122717	0.105090	—	0.104324	—	0.103679	—	0.103932	—	
	6	—	—	0.119944	—	0.119656	—	0.119826	—	0.119782	
	6[1)]	—	—	0.124097	—	0.122433	—	0.121662	—	0.120932	

[1)] With $\bar{w}_{nn} = 0$ imposed at plate boundary nodes

Table 5. Percentage errors in HT p-elements results displayed on Table 4

Quantity	N (DOF at el. corners)	Number of lines and columns of element stiffness matrix								
		16	24	28	32	36	40	44	48	52
Δw_C %	1	10.64	3.74	—	1.67	—	0.98	—	0.55	—
	3	-4.05	-0.78	—	-0.23	—	-0.10	—	-0.03	—
	6	—	—	-0.28	—	-0.10	—	-0.03	—	0.00
	6[1)]	—	—	-0.35	—	-0.13	—	-0.05	—	-0.02
ΔV_A %	1	-67.16	-41.55	—	-37.21	—	-32.44	—	-28.51	—
	3	0.67	-13.79	—	-14.42	—	-14.95	—	-14.74	—
	6	—	—	-1.61	—	-1.85	—	-1.71	—	-1.74
	6[1)]	—	—	1.80	—	0.43	—	-0.28	—	-0.80

[1)] With $\tilde{w}_{nn} = 0$ imposed at plate boundary nodes

3.2.3. Sensitivity to mesh distortion

The square simply supported and uniformly loaded plate from the two previous paragraphs was solved with the strongly distorted 2×2 FE mesh shown in Fig. 6b. The percentage errors displayed on Tables 12 (nodal averages) and 13 (results from auxiliary frame field) show that the solution is nearly insensitive to mesh distortion. This feature, typical for all HT elements [6, 7, 8, 9, 10], is mainly due to the fact that the internal Trefftz field of each element is defined in its local Cartesian coordinate system, independent of the mesh distortion. Note also that the elements with a single DOF at corner nodes are as unaffected by the mesh distortion as the ones with 3 or 6 DOF at corner nodes.

3.2.4. Error distribution over element area

One of the typical properties of the HT elements is the way in which the error in energy density ΔU_0, is distributed over the element area. In the case of Kirchhoff's thin plate

$$\Delta U_0 = \frac{1}{2D\,(1-\nu^2)} \left[\Delta M_x^2 - 2\nu \Delta M_x \Delta M_y + \Delta M_y^2 + 2\,(1+\nu)\,\Delta M_{xy}^2\right], \tag{34}$$

where

$$\Delta M = M_{\mathrm{FE}} - M_{\mathrm{EX}} \tag{34a}$$

and where M_{FE} and M_{EX} stand respectively for the FE approximation and the exact results. This error is known to be concentrated along the element boundary and to reach its maximum at the element corners — a distribution typical for the boundary solution approaches. In order to study the influence of the displacement frame formulation on this distribution, the uniformly loaded simply supported square plate was discretized by a single HT p-element extending over the whole plate area and solved in turn with the three alternative frame definitions from Section 2.3. The optional number M of side-mode DOF was fixed at 9 for $N = 1$, 7 for $N = 3$ and at 3 respectively 5 for $N = 6$. This choices lead to a 40×40 element stiffness matrix if $N = 1$ or 3 and to a 36×36 respectively 44×44 element stiffness matrix if $N = 6$. The corresponding distributions of the relative energy density error defined as

$$\varepsilon_0 = \frac{\Delta U_0}{U_{\mathrm{EX}}/\Omega} \tag{35}$$

(U_{EX}/Ω — average energy density equal to $0.0008512552623592293\ p^2L^4/D$ from series solution [25] with 20000 terms) were displayed in Fig. 7. These results clearly show the superior performance of the elements with $N = 6$ DOF at corner nodes. Although with $M = 5$ the total number of

Table 6. Centrally loaded simply supported square plate. 2 × 2 HT p-elements mesh (Fig. 6a) used over whole plate. Central load assumed uniformly distributed over circular area with radius $b = L/1000$ (load term (17a,b))

Quantity	N (DOF at el. corners)	Number of lines and columns of element stiffness matrix									Exact
		16	24	28	32	36	40	44	48	52	
$\frac{10Dw_C}{Pa^2}$	1	0.116544	0.116278	—	0.116133	—	0.116053	—	0.116032	—	0.1160084
	3	0.111704	0.115013	—	0.115635	—	0.115829	—	0.115911	—	
	6	—	—	0.115594	—	0.115813	—	0.115902	—	0.115946	
	6[1)]	—	—	0.115550	—	0.115798	—	0.115896	—	0.115943	
$\frac{V_A}{P}$	1	0.113772	0.122840	—	0.119159	—	0.120250	—	0.121488	—	0.1219053
	3	0.144929	0.129124	—	0.126481	—	0.124126	—	0.122715	—	
	6	—	—	0.120907	—	0.121054	—	0.121546	—	0.121688	
	6[1)]	—	—	0.123157	—	0.122155	—	0.122038	—	0.121904	

[1)] With $\tilde{w}_{nn} = 0$ imposed at plate boundary nodes

Table 7. Percentage error in HT p-elements results displayed on Table 6

Quantity	N (DOF at el. corners)	Number of lines and columns of element stiffness matrix								
		16	24	28	32	36	40	44	48	52
Δw_C %	1	0.46	0.23	—	0.11	—	0.04	—	0.02	—
	3	-3.71	-0.86	—	-0.32	—	-0.15	—	-0.08	—
	6	—	—	-0.36	—	-0.17	—	-0.09	—	-0.05
	6[1)]	—	—	-0.40	—	-0.18	—	-0.10	—	-0.06
ΔV_A %	1	-6.67	0.77	—	-2.25	—	-1.36	—	-0.34	—
	3	18.89	5.92	—	3.75	—	1.82	—	0.66	—
	6	—	—	-0.82	—	-0.70	—	-0.29	—	-0.18
	6[1)]	—	—	1.03	—	0.20	—	0.11	—	0.00

[1)] With $\tilde{w}_{nn} = 0$ imposed at plate boundary nodes

equations ($N_{\mathrm{Eqn}} = 16$) is smaller than that ($N_{\mathrm{Eqn}} = 20$) exhibited in the case of $N = 1$ with $M = 9$ or $N = 3$ with $M = 7$, the boundary error (in particular the error at the element corners) has been considerably attenuated. It is also interesting to observe that the solution $N = 6$ with $M = 3$ produced the same results as $N = 3$ with $M = 7$, but with only 12 equations instead of 16.

Further results for uniform and concentrated central load (load term (17a,b) used again with $b = L/1000$) were summarized on Tables 14 and 15 (points A, B and C as in Fig. 6). They show in particular that although a single element was used, the accuracy at the centre point C is now better than that of the nodal averages (Tables 3 and 7) with a 2×2 HT p-element mesh.

3.2.5. Comparison of computational effort for given accuracy in relative energy error norm

Since the cost of generating the element matrices $\overset{\circ}{\mathbf{r}}$ and $\mathbf{k}$ is largely problem dependent (the FE mesh in typical practical applications may comprise a more or less important number of resembling elements), this study takes into consideration only the computational effort necessary for solving the resulting system of linear equations. Though large differences exist between the performances of various equations solvers, this effort is usually assumed to be proportional to

$$\alpha = N_{\mathrm{Eqn}} B^2 , \tag{36}$$

where N_{Eqn} and B stand, respectively, for the number of equations and the half band width of the equation system. It is assumed that N_{Eqn} and B do not contain the DOF imposed at support points.

The h- and p- convergence in relative energy error norm defined as

$$\|e\| = \left(\frac{|U_{\mathrm{EX}} - U_{\mathrm{FE}}|}{U_{\mathrm{EX}}} \right)^{1/2} \tag{37}$$

was studied in terms of α for the classical problem of simply supported uniformly loaded square plate. The results displayed in logarithmic scale (base 10) in Fig. 8 to 11 show that for all types of displacement frames (1, 3 or 6 DOF at element corners) the crudest mesh, consisting in a single element over the whole plate, is the best in the present case. It is also interesting to point out that in the case of one or three DOF at element corners the h-convergence is much slower in terms of $\alpha = N_{\mathrm{Eqn}} B^2$ than the p-convergence (Fig. 8 and 9). This difference is considerably attenuated in the case of 6 DOF at element corners (Fig. 10 and 11).

In order to assess the computational effectivity of the three alternative displacement frames, Table 16 displays for several fixed values of the relative energy error norm $\|e\|$ the corresponding value of the measure of computational effort, $\alpha = N_{\mathrm{Eqn}} B^2$. This study makes it clear that the elements with 6 DOF at corners are the best and the ones with 1 DOF at corners the worst. The study of p-convergence of a centrally loaded plate in Fig. 12 also leads to a similar conclusion.

Table 8. Simply supported uniformly loaded square plate. Uniform 2 × 2 mesh of HT p-elements over whole plate (Fig. 6a). Results of uniform p-extension evaluated from nodal parameters at element's corners

Quantity	N (DOF at el. corners)	Number of lines and columns of element stiffness matrix									Exact
		16	24	28	32	36	40	44	48	52	
$\frac{10^2 D\tilde{w}_C}{pL^4}$	1	0.404499	0.405828	—	0.406312	—	0.406234	—	0.406237	—	0.406235
	3	0.408718	0.405796	—	0.406242	—	0.406234	—	0.406235	—	
	6	—	—	0.406253	—	0.406233	—	0.406234	—	0.406235	
	6[1)]	—	—	0.406257	—	0.406233	—	0.406234	—	0.406235	
$\frac{10\tilde{M}_{xC}}{pL^2}$	6	—	—	0.483364	—	0.478606	—	0.478558	—	0.478694	0.478864
	6[1)]	—	—	0.483386	—	0.478474	—	0.478491	—	0.478686	
$\frac{10\tilde{V}_A}{pL^2}$	6	—	—	0.658519	—	0.652386	—	0.650727	—	0.650202	0.649662
	6[1)]	—	—	0.658224	—	0.652458	—	0.650759	—	0.650206	

[1)] With $\tilde{w}_{nn} = 0$ imposed at plate boundary nodes

Table 9. Percentage errors in HT p-element results displayed on Table 8 (results of uniform p–extention evaluated from nodal parameters at element's corners

Quantity	N (DOF at el. corners)	Number of lines and columns of element stiffness matrix								
		16	24	28	32	36	40	44	48	52
$\Delta\tilde{w}_C$ %	1	-0.43	-0.10	—	0.02	—	0.00	—	0.00	—
	3	0.61	-0.11	—	0.00	—	0.00	—	0.00	—
	6	—	—	0.00	—	0.00	—	0.00	—	0.00
	6[1)]	—	—	0.01	—	0.00	—	0.00	—	0.00
$\Delta\tilde{M}_{xC}$ %	6	—	—	0.94	—	-0.05	—	-0.06	—	-0.04
	6[1)]	—	—	1.04	—	-0.08	—	-0.08	—	-0.04
$\Delta\tilde{V}_A$ %	6	—	—	1.36	—	0.42	—	0.16	—	0.08
	6[1)]	—	—	1.32	—	0.43	—	0.17	—	0.08

[1)] With $\tilde{w}_{nn} = 0$ imposed at plate boundary nodes

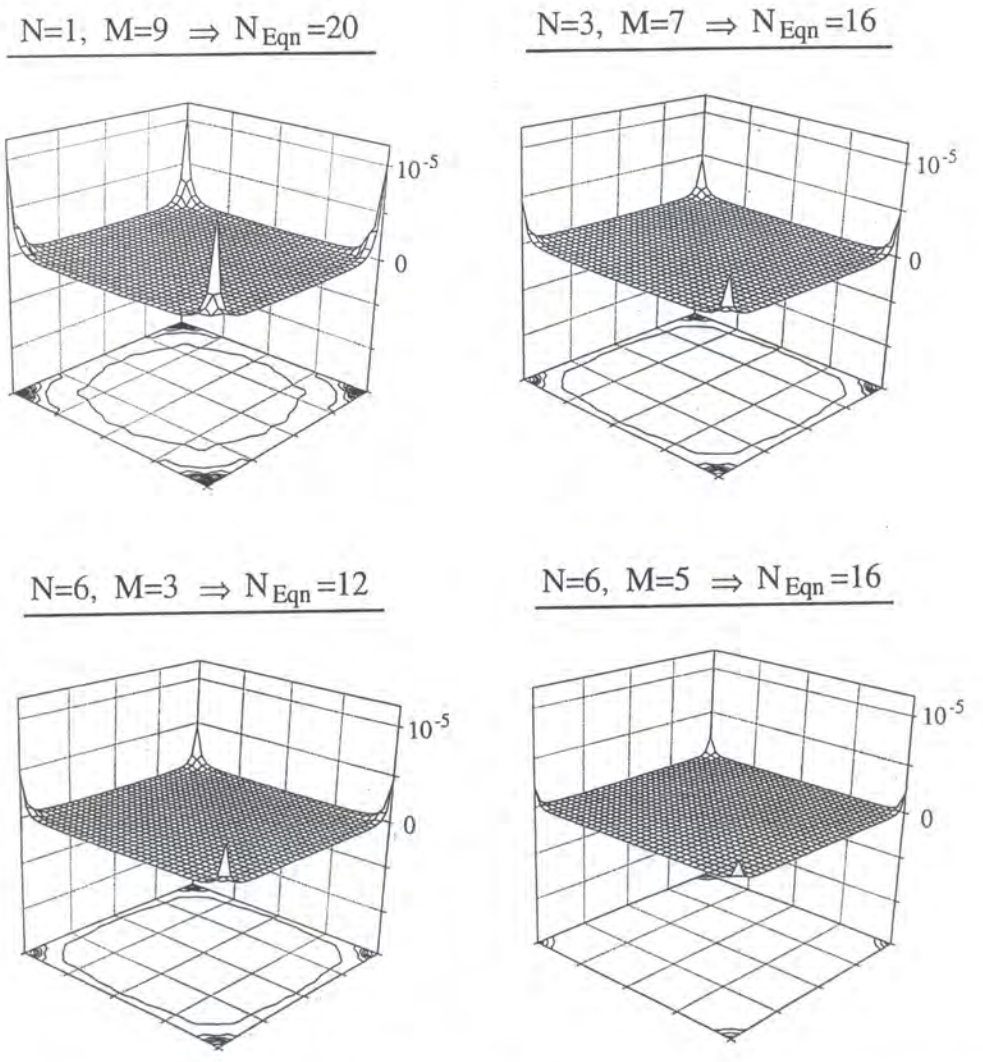

Fig. 7. Uniformly loaded simply supported plate. Distribution of relative error in strain energy density ε_0 (35) obtained with single element over whole plate for different numbers of corner (N) and side-mode (M) DOF. Level of first contour line = 0.8×10^{-6}, step between two subsequent conour lines = 2.0×10^{-6}

Table 10. Centrally loaded simply supported square plate. 2×2 HT p-elements mesh (Fig. 3a) used over whole plate. Central load assumed uniformly distributed over circular area with radius $b = L/1000$ (load term (17a,b)). Results evaluated from frame function field

Quantity	N (DOF at el. corners)	Number of lines and columns of element stiffness matrix									Exact
		16	24	28	32	36	40	44	48	52	
$\frac{10D\tilde{w}_C}{PL^2}$	1	0.116333	0.116380	—	0.116131	—	0.116059	—	0.116032	—	0.1160084
	3	0.111146	0.114927	—	0.115612	—	0.115820	—	0.115907	—	
	6	—	—	0.115559	—	0.115800	—	0.115897	—	0.115943	
	6[1)]	—	—	0.115512	—	0.115783	—	0.115891	—	0.115940	
$\frac{\tilde{V}_A}{P}$	6	—	—	0.118745	—	0.121481	—	0.121393	—	0.121609	0.1219053
	6[1)]	—	—	0.122159	—	0.123758	—	0.122863	—	0.122678	

[1)] With $\tilde{w}_{nn} = 0$ imposed at plate boundary nodes

Table 11. Percentage errors in HT p-elements results displayed on Table 10

Quantity	N (DOF at el. corners)	Number of lines and columns of element stiffness matrix								
		16	24	28	32	36	40	44	48	52
$\Delta\tilde{w}_C$ %	1	0.28	0.32	—	0.11	—	0.04	—	0.02	—
	3	-4.19	-0.93	—	-0.34	—	-0.16	—	-0.09	—
	6	—	—	-0.39	—	-0.18	—	-0.10	—	-0.06
	6[1)]	—	—	-0.43	—	-0.19	—	-0.10	—	-0.06
$\Delta\tilde{V}_A$ %	6	—	—	-2.59	—	-0.35	—	-0.34	—	-0.24
	6[1)]	—	—	0.21	—	1.52	—	0.79	—	0.63

[1)] With $\tilde{w}_{nn} = 0$ imposed at plate boundary nodes

Table 12. Percentage errors in nodal averages for simply supported uniformly loaded square plate solved with strongly distorted 2×2 HT p-elements mesh (Fig. 6b). Corresponding percentage errors for uniform 2×2 mesh (Fig. 6a) were shown on Table 3

Quantity	N (DOF at el. corners)	Number of lines and columns of element stiffness matrix								
		16	24	28	32	36	40	44	48	52
Δw_C %	1	0.17	0.02	—	-0.01	—	0.00	—	0.00	—
	3	0.77	-0.06	—	-0.01	—	0.00	—	0.00	—
	6	—	—	-0.01	—	0.00	—	0.00	—	0.00
	6[1)]	—	—	-0.01	—	0.00	—	0.00	—	0.00
ΔM_{xC} %	1	25.29	2.17	—	0.42	—	0.16	—	0.08	—
	3	4.77	0.01	—	-0.05	—	0.04	—	0.06	—
	6	—	—	-0.65	—	-0.12	—	-0.04	—	-0.04
	6[1)]	—	—	-0.72	—	-0.18	—	-0.03	—	-0.04
ΔM_{yC} %	1	32.13	6.21	—	0.95	—	-0.11	—	-0.08	—
	3	4.63	-0.69	—	-0.38	—	-0.29	—	-0.10	—
	6	—	—	-0.19	—	-0.19	—	-0.07	—	-0.02
	6[1)]	—	—	-0.17	—	-0.27	—	-0.07	—	-0.03
ΔQ_{yB} %	1	-4.32	-2.16	—	0.71	—	-0.76	—	0.31	—
	3	-4.66	-6.45	—	0.31	—	-0.90	—	0.13	—
	6	—	—	-3.35	—	0.08	—	-0.03	—	0.07
	6[1)]	—	—	-1.62	—	0.14	—	-0.17	—	0.16
ΔV_A %	1	-0.15	5.41	—	-1.88	—	-0.37	—	-0.33	—
	3	5.57	-0.36	—	0.00	—	-0.18	—	-0.16	—
	6	—	—	0.02	—	-0.06	—	-0.01	—	0.00
	6[1)]	—	—	-0.08	—	-0.05	—	-0.01	—	0.00

[1)] With $\tilde{w}_{nn} = 0$ imposed at plate boundary nodes

Table 13. Percentage errors in results derived from auxiliary frame field for simply supported uniformly loaded square plate solved with strongly distorted 2 × 2 HT p-elements mesh (Fig. 6b). Corresponding percentage errors for uniform 2 × 2 mesh (Fig. 6a) were shown on Table 9

Quantity	N (DOF at el. corners)	Number of lines and columns of element stiffness matrix								
		16	24	28	32	36	40	44	48	52
$\Delta\tilde{w}_C$ %	1	-3.70	0.02	—	-0.02	—	0.00	—	0.00	—
	3	0.82	-0.05	—	-0.01	—	0.00	—	0.00	—
	6	—	—	-0.01	—	0.00	—	0.00	—	0.00
	6[1)]	—	—	-0.01	—	0.00	—	0.00	—	0.00
$\Delta\tilde{M}_{xC}$ %	6	—	—	-0.68	—	-0.22	—	-0.08	—	-0.03
	6[1)]	—	—	-0.78	—	-0.35	—	-0.07	—	-0.05
$\Delta\tilde{M}_{yC}$ %	6	—	—	-0.30	—	-0.18	—	-0.07	—	-0.02
	6[1)]	—	—	-0.27	—	-0.29	—	-0.06	—	-0.04
$\Delta\tilde{V}_A$ %	6	—	—	1.41	—	0.48	—	0.21	—	0.12
	6[1)]	—	—	1.26	—	0.49	—	0.22	—	0.12

[1)] With $\tilde{w}_{nn} = 0$ imposed at plate boundary nodes

Table 14. Uniformly loaded simply supported square plate. Percentage errors in results obtained with single element extending over whole plate

Quantity	N (DOF at el. corners)	Number of lines and columns of element stiffness matrix								
		16	24	28	32	36	40	44	48	52
Δw_C %	1	19.66	-0.18	—	-0.04	—	0.00	—	0.00	—
	3	3.82	-0.13	—	-0.01	—	0.00	—	0.00	—
	6	—	—	-0.01	—	0.00	—	0.00	—	0.00
ΔM_{xC} %	1	13.12	-0.05	—	-0.07	—	0.00	—	0.00	—
	3	2.48	-0.01	—	-0.02	—	0.00	—	0.00	—
	6	—	—	-0.02	—	0.00	—	0.00	—	0.00
ΔQ_{yB} %	1	-25.96	4.60	—	2.38	—	-0.97	—	-0.67	—
	3	-29.96	3.79	—	1.89	—	-0.28	—	-0.42	—
	6	—	—	1.89	—	-0.28	—	-0.42	—	-0.09
ΔV_A %	1	39.69	-13.51	—	5.56	—	-3.57	—	1.11	—
	3	32.21	-12.19	—	2.35	—	-1.76	—	0.51	—
	6	—	—	2.35	—	-1.76	—	0.51	—	-0.21

Table 15. Centrally loaded simply supported square plate. Percentage errors in results obtained with single element extending over whole plate

Quantity	N (DOF at el. corners)	Number of lines and columns of element stiffness matrix								
		16	24	28	32	36	40	44	48	52
Δw_C %	1	8.45	0.06	—	0.05	—	0.00	—	0.00	—
	3	1.72	-0.36	—	0.01	—	0.00	—	0.00	—
	6	—	—	0.01	—	0.00	—	0.00	—	0.00
ΔQ_{yC} %	1	-23.72	-3.89	—	-3.51	—	-0.47	—	-0.49	—
	3	-23.72	12.59	—	-1.98	—	2.22	—	-0.26	—
	6	—	—	-1.98	—	2.22	—	-0.26	—	-0.27
ΔV_A %	1	17.81	7.03	—	4.90	—	-1.73	—	-1.90	—
	3	24.95	-10.75	—	-2.27	—	2.97	—	0.15	—
	6	—	—	-2.27	—	2.97	—	0.15	—	-0.60

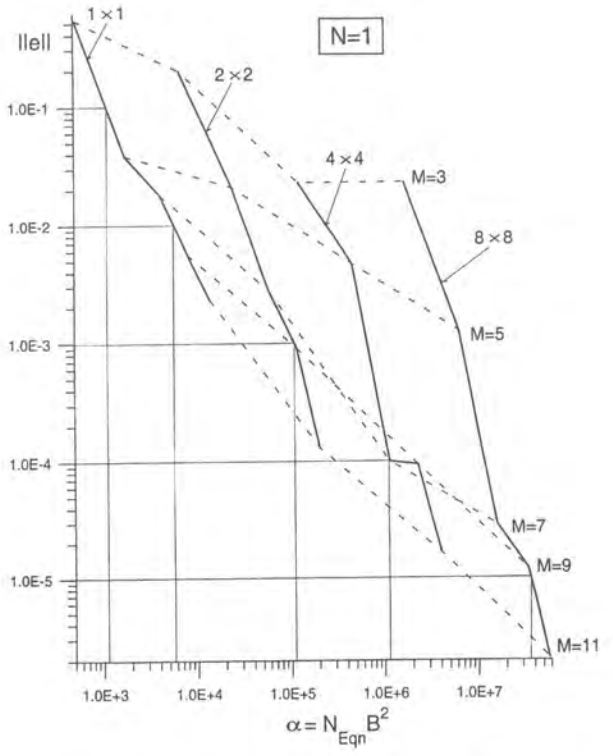

Fig. 8. Simply supported uniformly loaded square plate. Study of h- and p-convergence in relative energy error norm (37) as a function of measure of computational effort (36). Indicated density (from 1×1 to 8×8) concerns uniform HT-element mesh extending over whole plate

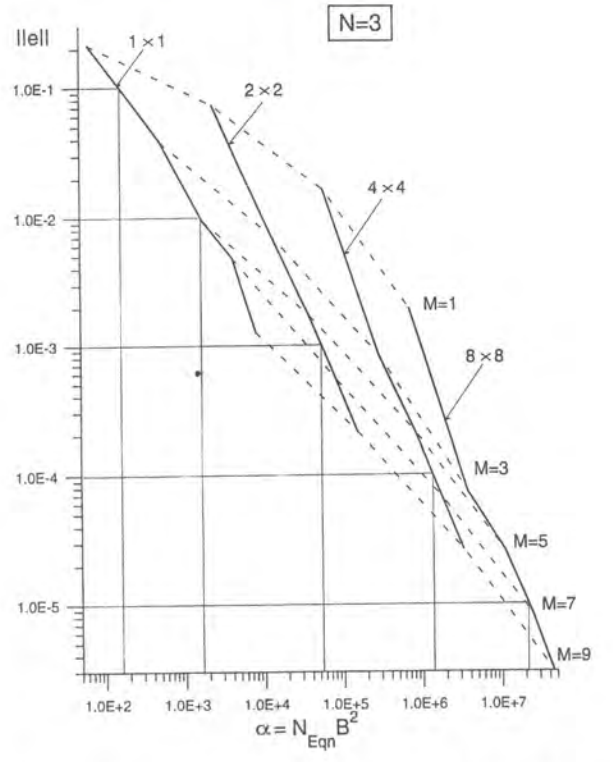

Fig. 9. Simply supported uniformly loaded square plate. Study of h- and p-convergence in relative energy error norm (37) as a function of measure of computational effort (36). Indicated density (from 1×1 to 8×8) concerns uniform HT-element mesh extending over whole plate

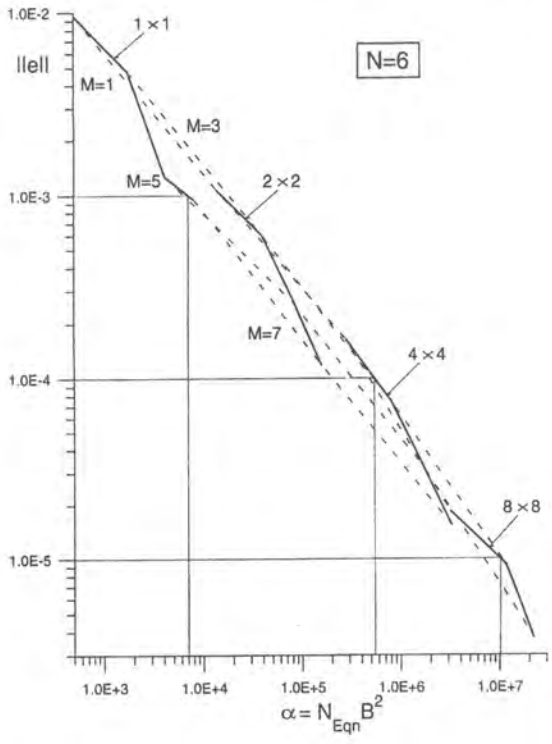

Fig. 10. Simply supported uniformly loaded square plate. Study of h- and p-convergence in relative energy error norm (37) as a function of measure of computational effort (36). Indicated density (from 1×1 to 8×8) concerns uniform HT-element mesh extending over whole plate

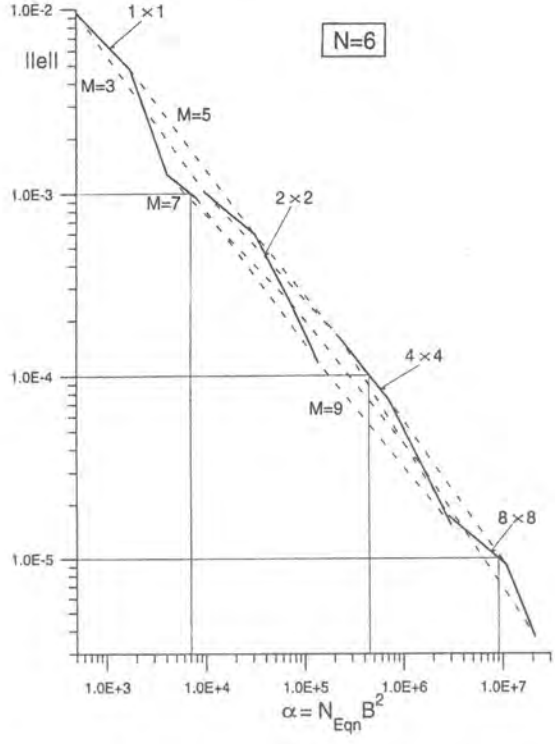

Fig. 11. Simply supported uniformly loaded square plate. Study of h- and p-convergence in relative energy error norm (37) as a function of measure of computational effort (36). Alternative solution with explicitely imposed condition $\tilde{w}_{nn} = 0$ at boundary nodes. Indicated density (from 1×1 to 8×8) concerns uniform HT-element mesh extending over whole plate

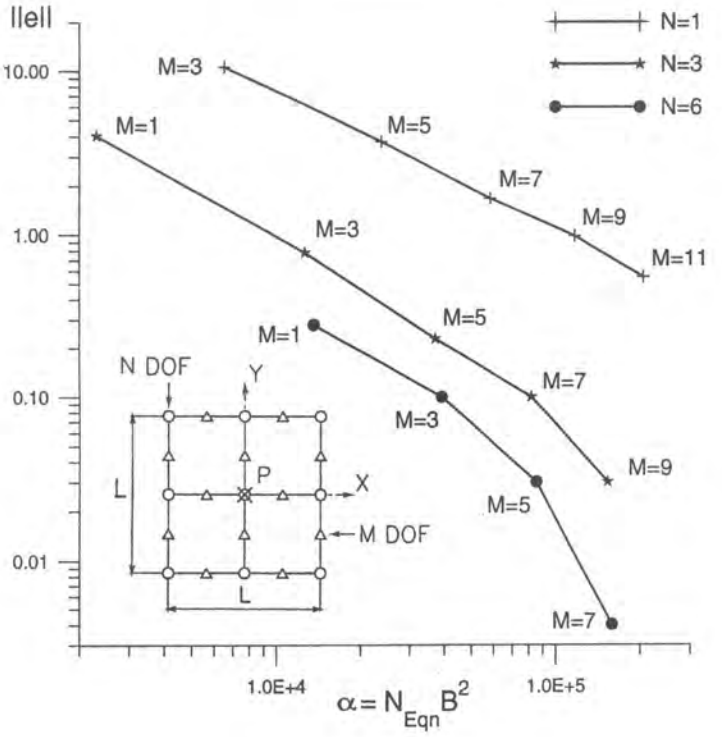

Fig. 12. Simply supported centrally loaded square plate. Study of p-convergence in relative energy error norm (37) as a function of measure of computational effort (36). Uniform 2 × 2 mesh of HT-p elements with 1, 3 or 6 DOF at corners nodes. As in conventional FEM, concentrated load P considered as nodal load

Table 16. Simply supported uniformly loaded square plate. Comparison of measure of computational effort (36) for specified values of relative energy error norm (37). Indicated mesh densities (from 1 × 1 to 8 × 8) concern uniform HT-element meshes extending over whole plate

FE mesh	$\|\|e\|\|$	$\alpha = N_{Eqn} B^2$			
		$N = 6^{1)}$	$N = 6$	$N = 3$	$N = 1$
1 × 1	10^{-1}	—	—	0.153×10^3	0.113×10^4
	10^{-2}	0.504×10^3	0.504×10^3	0.153×10^4	0.568×10^4
2 × 2	10^{-3}	0.100×10^5	0.161×10^5	0.518×10^5	0.107×10^6
4 × 4	10^{-4}	0.458×10^6	0.554×10^6	0.126×10^7	0.111×10^7
8 × 8	10^{-5}	0.900×10^7	0.100×10^8	0.200×10^8	0.364×10^8

[1)] With $\tilde{w}_{nn} = 0$ imposed at plate boundary nodes

3.3. Morley's skew plate

One of the most frequently used benchmark singularity problem is the analysis of the simply supported and uniformly loaded rhombic plate (Fig. 13). At the obtuse corners of 150°, this plate exhibits a very strong singularity with the exponent $\lambda = 6/5$ of the leading singularity term $Cr^{\lambda}\Phi(\vartheta)$ and reliable results by the standard FE calculation are difficult to reach [26]. The assessment of the three alternative displacement frames was based here on the comparison of numerical results for the transverse displacement w and the moments M_x and M_y at the plate center.

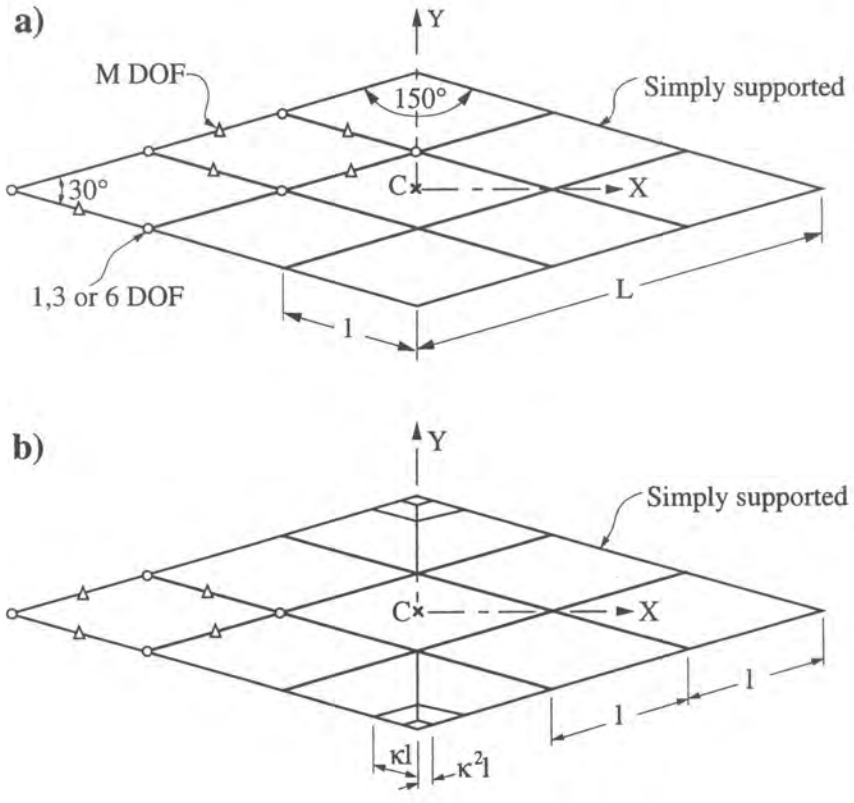

Fig. 13. Morley's rhombic plate: a) uniform 3×3 HT p-element mesh, b) locally refined HT-p element mesh

3.3.1. Solutions with uniform 3×3 HT-element mesh (Fig. 13a)

The results of the p-extension process and the corresponding percentage errors are displayed on Tables 17 and 18. The use of the 6 DOF at the element corners presents a particular problem for the specification of boundary conditions at the obtuse corners of the plate. Indeed, the standard specification

$$\tilde{w} = \frac{\partial \tilde{w}}{\partial x} = \frac{\partial \tilde{w}}{\partial y} = \frac{\partial^2 \tilde{w}}{\partial x^2} = \frac{\partial^2 \tilde{w}}{\partial y^2} = 0 \tag{38a}$$

leads here to $\tilde{M}_x = \tilde{M}_y = 0$, which is in sharp disagreement with the exact solution where $\tilde{M}_x$ tends to $+\infty$ and $\tilde{M}_y$ to $-\infty$ at these points. Therefore, as an alternative, the conditions

$$\tilde{w} = \frac{\partial \tilde{w}}{\partial x} = \frac{\partial \tilde{w}}{\partial y} = 0 \tag{38b}$$

was also considered. In this case, however, it was necessary to tolerate a non-vanishing displacement $\tilde{w}$ along the two element sides forming the angular corner. Neither of these two alternative possibilities was satisfactory on a crude uniform FE mesh. Indeed the errors (Table 18) were much larger than with 1 or 3 DOF at corner nodes. But the condition (38b) may be expected to improve the solution considerably on a locally refined mesh where the influence of the undesired boundary displacement, due to non-vanishing second order parameters at the obtuse corners, will be sensibly reduced due to the considerably decreased size of the two obtuse corner elements.

The observed lack of convergence (Table 18) of the solutions with either 1 or 6 DOF at element corners resembles the pollution error arising in the presence of a strong singularity, which is well

Table 17. Uniformly loaded simply supported Morley's 30° rhombic plate. Results at plate center for uniform 3 × 3 FE mesh (Fig. 13a)

Quantity	N (DOF at el. corners)	Number of lines and columns of element stiffness matrix							Exact
		16	24	28	32	36	40	44	
$\frac{10^2 D w_C}{pL^4}$	1	0.443870	0.434663	—	0.430303	—	0.428185	—	0.407845
	3	0.346805	0.386003	—	0.400472	—	0.408951	—	
	6[a)]	—	—	0.259521	—	0.292828	—	0.313201	
	6[b)]	—	—	0.416267	—	0.462034	—	0.492097	
$\frac{10 M_{xC}}{pL^2}$	1	0.115734	0.118643	—	0.117752	—	0.116861	—	0.108573
	3	0.078648	0.097744	—	0.106438	—	0.110454	—	
	6[a)]	—	—	0.043593	—	0.062660	—	0.072559	
	6[b)]	—	—	0.094956	—	0.119551	—	0.123184	
$\frac{10 M_{yC}}{pL^2}$	1	0.211253	0.198563	—	0.197325	—	0.196480	—	0.190620
	3	0.155192	0.178720	—	0.186121	—	0.189685	—	
	6[a)]	—	—	0.147772	—	0.158244	—	0.163580	
	6[b)]	—	—	0.179927	—	0.189672	—	0.197210	

[a)] With conditions (38a) at obtuse corners

[a)] With conditions (38b) at obtuse corners

Table 18. Uniformly loaded simply supported Morley's 30° rhombic plate. Percentage errors at plate center for uniform 3 × 3 FE mesh (Fig. 13a)

Quantity	N (DOF at el. corners)	Number of lines and columns of element stiffness matrix						
		16	24	28	32	36	40	44
Δw_C %	1	8.83	6.58	—	5.51	—	4.99	—
	3	-14.97	-5.36	—	-1.81	—	0.27	—
	$6^{a)}$	—	—	-36.37	—	-28.20	—	-23.21
	$6^{b)}$	—	—	2.07	—	13.28	—	20.66
ΔM_{xC} %	1	6.60	9.28	—	8.43	—	7.63	—
	3	-27.56	-9.97	—	-1.97	—	1.73	—
	$6^{a)}$	—	—	-59.85	—	-42.29	—	-33.17
	$6^{b)}$	—	—	-12.54	—	10.11	—	13.45
ΔM_{yC} %	1	10.82	4.17	—	3.52	—	3.07	—
	3	-18.59	-6.24	—	-2.36	—	-0.49	—
	$6^{a)}$	—	—	-22.48	—	-16.98	—	-14.19
	$6^{b)}$	—	—	-5.61	—	-0.50	—	3.46

$^{a)}$ With conditions (38a) at obtuse corners
$^{a)}$ With conditions (38b) at obtuse corners

known from the conventional p-element analysis. In contrast, the solution with 3 DOF at element corners is surprisingly accurate. Indeed, with 7 DOF at mid-side nodes (a 40×40 element stiffness matrix) and without the use of any tricks, the errors at plate center (Table 18) are inferior to 2%.

3.3.2. Solution with locally refined HT-element mesh (Fig. 13b)

As in the case of conventional p-elements [27], the obtuse corners were isolated by two layers of small elements graded towards the singularity following the geometrical progression with a common factor $\kappa = 0.15$. All results (Tables 19 and 20) were considerably improved as compared to those obtained with a uniform 3×3 mesh. The elements with 3 DOF at corners gave again excellent results. With 7 DOF at mid-side nodes the maximal error in moments at the plate center was only 0.25%. As expected, excellent results, but with a slightly larger element stiffness matrix (44×44 for $M = 5$), were also obtained with the elements with 6 DOF at element corners when the conditions (38b) were applied at the obtuse corners of the plate. On the other hand, the results obtained with the conditions (38a) were the worst of all considered solutions. Indeed with the error of 6.12% in M_x, this solution was worse than that with 3 DOF at element corners on a uniform 3×3 element mesh (Table 18). The error of the solution with 1 DOF at element corners has been decreased by a factor of 4.1 to 10.6 as compared to results on a uniform 3×3 mesh, but these smaller errors do not seem to significantly improve with the order of the approximation.

Slightly better results than with $\kappa = 0.15$ have been obtained with $\kappa = 0.10$ (Table 21) while otherwise the observed behaviour of the uniform p-extension with the three alternative displacement frame formulations has remained unchanged.

4. Concluding remarks

In the hybrid-Trefftz formulation the elements are linked through an auxiliary displacement frame which is defined at the element boundary in terms of the same nodal parameters (and, in the case of the p-version elements, also the non-nodal side modes parameters) as used in the conventional assumed displacement elements.

Table 19. Uniformly loaded simply supported Morley's 30° rhombic plate. Results at plate center for locally refined FE mesh (Fig. 13b) with $\kappa = 0.15$

Quantity	N (DOF at el. corners)	Number of lines and columns of element stiffness matrix							Exact
		16	24	28	32	36	40	44	
$\frac{10^3 D w_C}{pL^4}$	1	0.411231	0.413640	—	0.412979	—	0.412448	—	0.407845
	3	0.399307	0.405054	—	0.407019	—	0.408664	—	
	6[a)]	—	—	0.382787	—	0.387057	—	0.390126	
	6[b)]	—	—	0.401149	—	0.405147	—	0.408229	
$\frac{10 M_{xC}}{pL^2}$	1	0.106851	0.110128	—	0.110763	—	0.110328	—	0.108573
	3	0.101886	0.108348	—	0.108321	—	0.108846	—	
	6[a)]	—	—	0.098681	—	0.100708	—	0.101933	
	6[b)]	—	—	0.105864	—	0.107467	—	0.108708	
$\frac{10 M_{yC}}{pL^2}$	1	0.195575	0.192014	—	0.192197	—	0.191940	—	0.190620
	3	0.184931	0.190250	—	0.190388	—	0.190862	—	
	6[a)]	—	—	0.183173	—	0.184610	—	0.185480	
	6[b)]	—	—	0.188614	—	0.189850	—	0.190739	

[a)] With conditions (38a) at obtuse corners

[a)] With conditions (38b) at obtuse corners

Table 20. Uniformly loaded simply supported Morley's 30° rhombic plate. Percentage errors at plate center for locally refined FE mesh (Fig. 13b) with $\kappa = 0.15$

Quantity	N (DOF at el. corners)	Number of lines and columns of element stiffness matrix						
		16	24	28	32	36	40	44
Δw_C %	1	0.83	1.42	—	1.26	—	1.13	—
	3	-2.09	-0.68	—	-0.20	—	0.20	—
	$6^{a)}$	—	—	-6.14	—	-5.10	—	-4.34
	$6^{b)}$	—	—	-1.64	—	-0.66	—	0.09
ΔM_{xC} %	1	-1.59	1.43	—	2.02	—	1.62	—
	3	-6.16	-0.21	—	-0.23	—	0.25	—
	$6^{a)}$	—	—	-9.11	—	-7.24	—	-6.12
	$6^{b)}$	—	—	-2.50	—	-1.02	—	0.12
ΔM_{yC} %	1	2.60	0.73	—	0.83	—	0.69	—
	3	-2.98	-0.19	—	-0.12	—	0.13	—
	$6^{a)}$	—	—	-3.91	—	-3.15	—	-2.70
	$6^{b)}$	—	—	-1.05	—	-0.40	—	0.06

$^{a)}$ With conditions (38a) at obtuse corners

$^{a)}$ With conditions (38b) at obtuse corners

Table 21. Uniformly loaded simply supported Morley's 30° rhombic plate. Percentage errors at plate center for locally refined FE mesh (Fig. 13b) with $\kappa = 0.10$

Quantity	N (DOF at el. corners)	Number of lines and columns of element stiffness matrix						
		16	24	28	32	36	40	44
Δw_C %	1	1.15	1.19	—	0.96	—	0.84	—
	3	-1.74	-0.44	—	-0.14	—	0.13	—
	$6^{b)}$	—	—	-1.17	—	-0.47	—	0.07
ΔM_{xC} %	1	-0.99	1.10	—	1.57	—	1.20	—
	3	-5.88	0.16	—	-0.15	—	0.15	—
	$6^{b)}$	—	—	-1.83	—	-0.74	—	0.09
ΔM_{yC} %	1	2.85	0.58	—	0.65	—	0.51	—
	3	-2.90	-0.02	—	-0.09	—	0.08	—
	$6^{b)}$	—	—	-0.75	—	-0.28	—	0.05

$^{a)}$ With conditions (38b) at obtuse corners

This study was dealing with the thin Kirchhoff plates in which case the role of the generalized displacement frame, consisting of transverse displacement $\tilde{w}$ and normal rotation $\tilde{\varphi}$, was the enforcement of the C^1 conformity on the internal Trefftz-type displacement field w of the element. While the standard frame is assumed to be exactly and minimally conforming [8, 18], which implies the use of 3 nodal parameters $(\tilde{w}, \tilde{w}_x, \tilde{w}_y)$ at the element corners, this limitation is not compulsory. Two alternative displacement frame formulations, with either 6 DOF $(\tilde{w}, \tilde{w}_x, \tilde{w}_y, \tilde{w}_{xx}, \tilde{w}_{xy}, \tilde{w}_{yy})$ or only a single DOF $(\tilde{w})$ at the element corners, were also investigated. While the former formulation may be qualified as overconforming (since, locally, the C^2 conformity is unnecessarily enforced at the element corners), the latter may be qualified as underconforming (since at the element corners the definition of the rotation components, $\tilde{w}_x$ and $\tilde{w}_y$, is no longer unique). The admissibility of such a frame is due to the fact that since no such default exists for the standard internal displacement field w, the matching process between w, w_x, w_y and $\tilde{w}, \tilde{w}_x, \tilde{w}_y$ indirectly tends to enforce the missing unicity condition on $\tilde{w}_x$ and $\tilde{w}_y$.

Each of the three investigated displacement frame formulations has been shown to possess specific advantages and shortcomings. For a given polynomial degree of the frame functions $\tilde{w}$ and $\tilde{\varphi}$, the frame with 1 DOF at corners necessitates the largest and the frame with 6 DOF the lowest total

number of DOF. Thus, for example, if the number of corner node DOF of a quadrilateral element with quintic $\tilde{w}$ and quartic $\tilde{\varphi}$ is respectively equal to 1, 3 and 6, then the total number, n, of its DOF is respectively equal to 40, 32 and 28. Therefore, it is not surprising that from the point of view of the computational effort for a given level of accuracy, the element with 6 DOF at corners is the best and the element with 1 DOF at corners the worst. To a similar conclusion has also led the study of the error distribution over the area of the element. Indeed, though in each of the three alternative frame formulations the largest errors always appear at the element corners, this error concentration appears to be the most severe for elements with one and the least severe with six DOF at corners. The additional advantage of the six DOF is also the possibility of direct evaluation of bending and twisting moments at the element corners from the second order DOF, $\tilde{w}_{xx}$, $\tilde{w}_{xy}$ and $\tilde{w}_{yy}$, and perhaps also the possibility of using the differences between these results and those obtained from element's internal field as an *a posteriori* error estimation (not yet investigated).

The above reported studies show in comparatively bad light the HT elements with a single DOF at corners. Clearly, the abandon of the corner nodes DOF, $\tilde{w}_x$ and $\tilde{w}_y$, accentuates the tendency of the HT elements to error concentration at the element corners and increases the cost of calculation necessary to reaching the required accuracy. However, these elements present an important advantage in that the definition of the auxiliary out-of-plane displacement field $\tilde{w}$ is the same as that used for the in-plane displacements $\tilde{u}$ and $\tilde{v}$ in the HT plane elasticity element formulation [6, 28]. This makes it possible to combine the in- and the out-of-plane formulations into a HT folded plate p-element [29] (Fig. 14) which possesses three global Cartesian displacement components $\left(\tilde{U}, \tilde{V}, \tilde{W}\right)$ at the element corners and an optional number of hierarchical side modes DOF for the normal rotation $\tilde{\varphi}$ and the higher order terms for the global Cartesian displacement components.

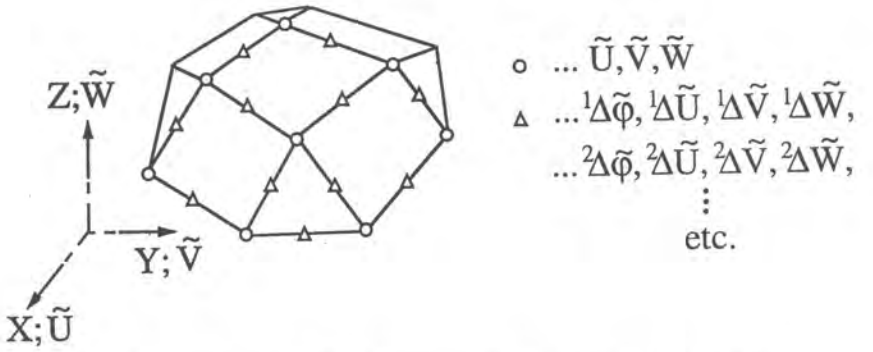

Fig. 14. Application of HT p-elements to analysis of folded plates

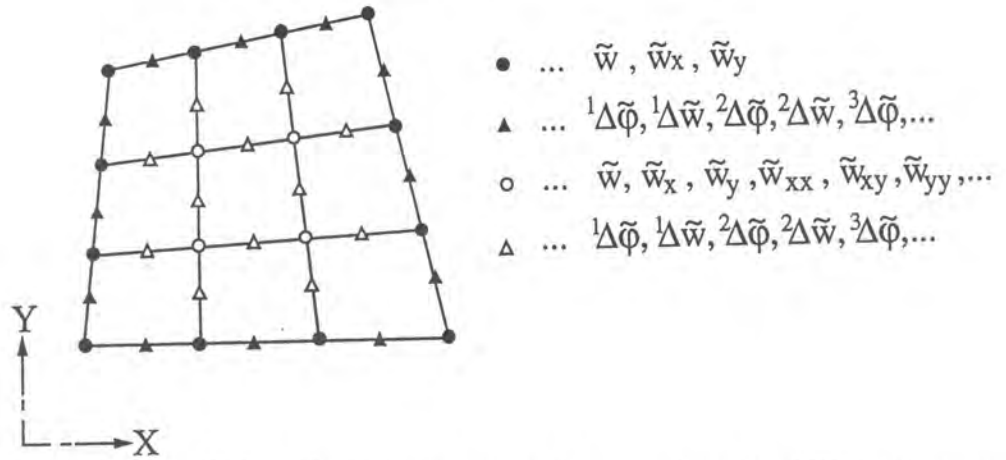

Fig. 15. Application of HT Kirchhoff plate p-elements with unequal number of DOF at element corner nodes: • – 3 DOF and o – 6 DOF

Provided that there are no jumps in the plate thickness and that the discontinuous loads are properly accounted for by an appropriate particular term (Sec. 2.2 and Ref. [13]), the only disadvantage of using 6 DOF at the element corners is that in some cases (such as the singular obtuse corner of a skew plate) it is not obvious how the higher order parameters $\tilde{w}_{xx}$, $\tilde{w}_{xy}$, $\tilde{w}_{yy}$ should be imposed. In order to retain the maximum of advantages of various alternative displacement frame formulations while discarding their drawbacks, the obvious solution consists (Fig. 15) in using 6 DOF at element corners inside the FE mesh along with 3 DOF (or 1 DOF) at nodes situated at the mesh boundary. The ease with which can be generated the corresponding frame functions makes this idea particularly tempting to investigate.

Acknowledgements

The research reported in this paper was partially supported by the KBN under Grant No. PB 0591/P4/94/06.

References

[1] E. Trefftz. Ein Gegenstück zum Ritzschen Verfahren. In: *Proceedings 2nd International Congress of Applied Mechanics*, Zurich, 131–137, 1926.

[2] J. Jirousek. Basis for development of large finite elements locally satisfying all field equations. *Comp. Meth. Appl. Mech. Eng.*, **14**: 65–92, 1978.

[3] T. H. Pian. Derivation of element stiffness matrices by assumed stress distributions. *AIAA Journal*, **2**: 1333–1336, 1964.

[4] J. Jirousek, A. Zieliński. *Survey of Trefftz-type element formulations.* Int Rep. LSC 95/06, Swiss Federal Institute of Technology, Lausanne, 1995. See also *Comp. Struct.*, **63**: 225–242, 1997.

[5] J. Jirousek, A. Wróblewski. T-elements: State of the art and future trends. *Archives of Comp. Meth. in Engng*, **3**: 323–434, 1996.

[6] J. Jirousek, P. Teodorescu. Large finite elements method for the solution of problems in the theory of elasticity. *Comp. Struct.*, **15**: 575–587, 1982.

[7] J. Jirousek, L. Guex. The hybrid–Trefftz finite element model and its application to plate bending. *Int. J. Numer. Meth. Eng.*, **23**: 651–693, 1986.

[8] J. Jirousek. Hybrid–Trefftz plate bending elements with p-method capabilities. *Int. J. Numer. Meth. Eng.*, **24**: 1367–1393, 1987.

[9] J. Jirousek, A. Venkatesh. Implementation of curvilinear geometry into p-version HT plate elements. *Int. J. Numer. Meth. Eng.*, **28**: 431–443, 1989.

[10] A. Venkatesh, J. Jirousek. *Accurate analysis of thin plates under concentrated loading.* IREM Int. Rep. 89/6, Swiss Federal Institute of Technology, Lausanne, June 1989.

[11] A. Venkatesh, J. Jirousek. Finite element formulation for the analysis of local effects. In: V. Krupka, M. Drdacky, eds., *Contact Loading and Local Effects in Thin Walled Plated and Shell Structures* , Berlin, Springer–Verlag, 1991.

[12] J. Jirousek, M. N'Diaye. Hybrid–Trefftz p-method elements for analysis of flat slabs with drops. *Comp. Struct.*, **43**: 163–179, 1992.

[13] A. Venkatesh, J. Jirousek. Accurate representation of local effect due to concentrated and discontineous loads in hybrid–Trefftz plate bending elements. *Comp. Struct.*, **57**: 863–870, 1995.

[14] J. Jirousek, A. P. Zieliński, H. Rabemanantsoa, A. Venkatesh. Study of two alternative p-element formulations. In: P. Ladeveze, O. C. Zienkiewicz, eds., *New Advances in Comp. Struc. Mech.* , 189–203, Elsevier, 1992.

[15] J. Jirousek, A. Venkatesh, A. P. Zieliński, H. Rabemantantsoa. Comparative study of p–extensions based on conventional assumed displacement and hybrid–Trefftz FE models. *Comp. Struct.*, **46**: 261–278, 1993.

[16] J. Jirousek, A. Venkatesh. A simple stress error estimator for hybrid–Trefftz p-version elements. *Int. J. Numer. Meth. Eng.*, **28**: 211–236, 1989.

[17] J. Jirousek, A. Venkatesh. Adaptivity in hybrid–Trefftz finite element formulation. *Int. J. Numer. Meth. Eng.*, **29**: 391–405, 1990.

[18] J. Jirousek, A. Venkatesh. A new FE approach for adaptive reliability assurance. *Comp. Struct.*, **37**: 217–230, 1990.

[19] J. Jirousek, B. Szybiński, A. Wróblewski. Mesh design and reliability assurance in hybrid–Trefftz p-element approach. *Finite elements in Analysis and Design*, **22**: 225–247, 1996.

[20] J. Jirousek. Variational formulation of two complementary hybrid–Trefftz FE models. *Comm. Numer. Meth. Eng.*, 837–845, 1993.

[21] A. P. Zieliński, O. C. Zienkiewicz. Generalized finite element analysis with T–complete boundary solution functions. *Int. J. Numer. Meth. Eng.*, **21**: 509–528, 1985.

[22] I. Herrera, *Boundary Methods – an Algebraic Theory.* Pitman Advanced Publishing Program, Boston – London – Melbourne, 1984.

[23] J. Jirousek. Structural analysis program SAFE – special features and advanced finite element models. *Adv. Eng. Software*, **7**: 68–76, 1985.

[24] D. Wang, I. Katz, B. Szabo. Implementation of C^1 triangular element based on p-version of the finite element method. *Comp. Struct.*, **19**: 381–392, 1984.

[25] H. Reismann. *Elastic Plates: Theory and Applications.* Wiley, New York, 1988.

[26] J. Robinson. An evaluation of skew sensitivity of thirty three plate bending elements in nineteen FEM systems. Finite Element News – Special Report, 1985.

[27] S. Szabo. Mesh design for the p-version of the finite element method. *Comp. Meth. Appl. Mech. Eng.*, **55**: 181–197, 1986.

[28] J. Jirousek, A. Venkatesh. Hybrid–Trefftz plane elasticity elements with p-method capabilities. *Int. J. Numer. Meth. Eng.*, **35**: 1443–1472, 1992.

[29] J. Jirousek, B. Szybiński, A. Zieliński. Application of hybrid Trefftz p-element to analysis of folded plates. In: *Proceedings XII Polish Conference on Computer Methods in Mechanics*, Warsaw–Zegrze, Poland, 146–148, 1995.